JCI insight

Multi-omic analysis of microRNA-mediated regulation reveals a proliferative axis involving miR-10b in fibrolamellar carcinoma

Adam B. Francisco, … , Nabeel Bardeesy, Praveen Sethupathy

JCI Insight. 2022. https://doi.org/10.1172/jci.insight.154743.

Research In-Press Preview Oncology

Graphical abstract

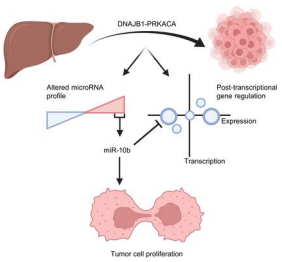

Multi-omic analysis of microRNA-mediated regulation reveals a proliferative axis involving miR-10b in fibrolamellar carcinoma

Adam B. Francisco[1], Matt Kanke[1], Andrew P. Massa[1], Timothy A. Dinh[1], Ramja Sritharan[1], Khashayar Vakili[2], Nabeel Bardeesy[3], Praveen Sethupathy[1]

[1]Department of Biomedical Sciences, College of Veterinary Medicine, Cornell University, Ithaca, NY, USA
[2]Department of Surgery, Boston Children's Hospital, Boston, MA, USA
[3]Department of Medicine, Harvard Medical School, Boston, MA, USA

Correspondence:
Praveen Sethupathy, PhD
Department of Biomedical Sciences
College of Veterinary Medicine
Cornell University
Veterinary Research Tower T7 006D
Ithaca, NY 14853
Email: pr46@cornell.edu
Telephone: 607-253-4347
Fax: 607-253-4447

Grant support
This work was supported by a grant from the Tisch Families' Faculty Development Fund (awarded to K.V.), a grant from the Boston Children's Hospital/ CMCH Surgical Foundation (awarded to K.V.), and a grant from the Fibrolamellar Carcinoma Foundation (awarded to P.S.).

Disclosures
The authors have no conflicts of interest exist to disclose.

Transcript Profiling
Gene Expression Omnibus accession numbers GSE181922 and GSE114974. European Genome-Phenome Archive accession number EGAS00001004169.

Synopsis
Small RNA profiling of the largest fibrolamellar carcinoma (FLC) patient cohort to date, coupled with genome-scale RNA and chromatin analysis, identifies miR-10b as a candidate master regulator of gene expression in FLC. Functional analysis of miR-10b in PDX-derived FLC cells demonstrates it is a regulator of tumor cell metabolic activity and proliferation.

Abstract

Background and Aims: Fibrolamellar carcinoma (FLC) is an aggressive liver cancer primarily afflicting adolescents and young adults. Patients with FLC harbor a heterozygous deletion on chromosome 19 that leads to the oncogenic gene fusion, *DNAJB1-PRKACA*. There are currently no effective therapeutics for FLC. To work toward that end, it is critical to gain deeper mechanistic insight into FLC pathogenesis.

Methods: We assembled a large sample set of FLC and non-malignant liver tissue (n=52) and performed integrative multi-omic analysis. Specifically, we carried out small RNA-sequencing to define altered microRNA expression patterns in tumor samples and then coupled this analysis with RNA sequencing (RNA-seq) and chromatin run-on sequencing (ChRO-seq) data to identify candidate master microRNA regulators of gene expression in FLC. We also evaluated the relationship between *DNAJB1-PRKACA* and microRNAs of interest in several human and mouse cell models. Finally, we performed loss-of-function experiments for a specific microRNA in cells established from a patient-derived xenograft (PDX) model.

Results: We identified miR-10b-5p and miR-455-3p as the top candidate pro-proliferative and tumor suppressive microRNAs, respectively. In multiple human cell models, but not in mouse cell models, over-expression of *DNAJB1-PRKACA* leads to significant up-regulation of miR-10b-5p. In cells established from a PDX model, inhibition of miR-10b increases the expression of several novel target genes, including the anti-proliferative factors *TRIM35* and *SUN2*, concomitant with a significant reduction in metabolic activity, anchorage-independent growth, and proliferation.

Conclusion: This functional genomics study highlights a novel proliferative axis in FLC and provides a rich resource for further investigation of the molecular landscape of FLC. The results reveal that miR-10b-5p shapes gene expression and promotes cell proliferation in FLC. Future studies are necessary to identify how the loss of miR-455-3p contributes to FLC progression and how miR-10b-5p may coordinate with miR-455-3p to control tumor phenotypes.

Keywords: cancer genomics, fibrolamellar carcinoma, microRNA, young adult and adolescent cancer, multi-omic analysis

Abbreviations

C, Celsius; cAMP, cyclic adenosine monophosphate; CDH1, Cadherin 1; ChRO-seq, chromatin run on sequencing; COAD, colon adenocarcinoma; CoV, coefficient of variation; CRISPR, clustered regularly interspaced short palindromic repeats; CTG, cell titer glo; DNAJB1, DnaJ Heat Shock Protein Family (Hsp40) Member B1; DP, DNAJB1-PRKACA; EdU, 5-ethynyl-2'-deoxyuridine; FANCC, Fanconi Anemia Complement Group C; FC, fold change; FCF, fibrolamellar cancer foundation; FLC, fibrolamellar carcinoma; GFP, green fluorescent protein; GPR, gain of post-transcriptional regulation; HB, hepatoblastoma; HCC, hepatocellular carcinoma; IOPN, intraductal oncocytic papillary neoplasm; isomiR, isoform of a microRNA; kb, kilobase; KLF11, Kruppel Like Factor 11; LNA, locked-nucleic acid inhibitor; LPR, loss of post-transcriptional regulation; miR, microRNA; MIM, locked-nucleic acid mimic, NML, non-malignant liver; nt, nucleotide; PCA, principal component analysis; PDX, patient derived xenograft; PKA or PRKACA, protein kinase A catalytic alpha subunit; PTR; post-transcriptional regulation; PTEN, phosphatase and tensin homolog; qPCR, quantitative polymerase chain reaction; RBP, RNA binding protein; READ, rectal adenocarcinoma; RNA, ribonucleic acid; RNA-seq, messenger RNA sequencing; RQV, relative quantitative value; SEC14L2, SEC14 Like Lipid Binding 2; SIRT5, Sirtuin 5; SUN2, Sad1 and UNC84 Domain Containing 2; TCGA, the cancer genome atlas; TUNEL, terminal deoxynucleotidyl transferase dUTP nick end labeling; TRIM35, Tripartite Motif Containing 35; TWIST1, Twist Family BHLH Transcription Factor 1; VST, variance stabilized transformed normalized counts; WT, wild-type.

Introduction

Fibrolamellar carcinoma (FLC) is a rare and aggressive type of liver cancer (1,2). FLC predominantly afflicts adolescent and young adults who lack features that are predisposing to other liver cancers, such as alcoholism, obesity, hepatitis or parasitic infections, and chronic exposure to toxins (3). Standard of care for typical liver cancer, referred to as hepatocellular carcinoma, has thus far not proven effective (4,5). The only current successful treatment option is surgical resection. Unfortunately, detection of FLC often doesn't occur until later stages of disease progression, and for patients with advanced metastatic cancer for whom resection is not a viable strategy, the prognosis is dismal (6-9). There is a dire need for effective therapies. To work toward this, it is critical to first understand the mechanisms underlying FLC progression.

Nearly all patients with FLC carry a heterozygotic deletion of ~400kb on chromosome 19 between the genes *DNAJB1* (encoding a small heat-shock factor) and *PRKACA* (encoding a catalytic subunit of the cAMP-dependent protein kinase holoenzyme PKA), which results in the creation of the in-frame fusion gene *DNAJB1-PRKACA* and the eventual expression of the protein chimera DNAJ-PKAc (DP) (10-12). DP is oncogenic in murine livers (13,14) and thought to be the driver of FLC formation. There is considerable interest in developing chemical inhibitors of DP activity; however, off-target suppression of PKA remains an unfavorable outcome due to the importance of PKA in the normal physiology of critical organs including the heart (15-17). Genome-scale analysis of FLC tumors has revealed reproducible changes in the expression of many genes (18-20), several of which have been shown to be strongly sensitive to DP activity (21,22). This finding prompts the hypothesis that genes downstream of DP may represent alternative therapeutic targets.

One class of genes shown to be altered in FLC is microRNAs (22,23), which are ~21-nt small RNAs that negatively regulate gene expression at the post-transcriptional level (24). Two initial studies identified dysregulated microRNAs but were under-powered in terms of the number of FLC tumor samples (18 in one study (22) and 7 in another (23)). In this study, we performed small RNA sequencing analysis in the largest set of FLC and non-malignant samples to date (n=52) and identified a set of significantly upregulated microRNAs in both primary and metastatic tumors. We found that miR-10b is among the most dramatically up-regulated in FLC. There was little difference overall between primary and metastatic microRNA expression profiles. We then leveraged our published FLC chromatin run-on sequencing (ChRO-seq) data to identify the transcriptional start sites and quantify transcriptional activity of the significantly upregulated microRNAs, which revealed that miR-10b is the most transcriptionally activated microRNA locus in FLC. We then performed an integrative analysis of ChRO-seq and RNA-seq datasets to identify those genes subject primarily to post-transcriptional regulation (PTR) in FLC. Among the PTR genes that are down-regulated in FLC, we observed a significant enrichment of predicted binding sites for miR-10b.

We found that the expression and activity of DP is sufficient to induce the up-regulation of miR-10b in multiple human, but not mouse, cell models of FLC, which points to important species-specific differences in terms of the downstream effects of DP. We then performed functional analysis of miR-10b in two FLC cell lines, independently derived from a patient derived xenograft (PDX). After inhibition of miR-10b, we observed a modest but significant reduction in cell metabolism, anchorage-independent growth, and proliferation, which associates with a significant increase in the expression of novel candidate target genes of miR-10b, *FANCC*, *SUN2* and *TRIM35*. All three of these genes have been implicated as tumor suppressors in other cancer types (25-32). Overall, our results reveal a regulatory axis in FLC involving miR-10b to promote cellular proliferation.

Results

MicroRNA profiling in the largest FLC and non-malignant liver sample set to date

Tissue samples from patients with FLC were acquired though a collaboration with the Fibrolamellar Cancer Foundation (FCF) biobank, resulting in a substantially expanded set (n=52, n=47 after removal of samples acquired from the same patient at a different time) relative to our prior analysis (22), which included only 18 samples. Patient samples were obtained at the time of surgical procedures, frozen, and stored at -80°C. When possible, nonmalignant liver (NML) adjacent to the FLC tumors was also obtained. We confirmed the presence of the DP oncogene in each sample by real-time quantitative PCR (RT-qPCR), detection of the fusion transcript in RNA-seq data, or Western blot (**Supplemental Table 1**). The expression of DP in samples analyzed by qPCR (**Figure 1A**) is on average ~1000-fold higher in FLC than in NML tissue. We also determined that the median age of the patients in our dataset is 21 years old (**Figure 1B**), consistent with the notion that FLC is primarily an adolescent and young adult cancer.

We extracted RNA from each patient sample and proceeded with small RNA-sequencing (Methods). After ensuring that all samples had a sufficient number of mapped reads (>1 million reads, Supplemental Table 2), we quantified microRNA expression using miRquant 2.0 (33). Principal component analysis (PCA) revealed that the microRNA expression profiles are sufficient to stratify samples according to NML and FLC status (**Figure 1C**), but not age or sex (**Figure 1D**), indicating that microRNA differences are due to tumor biology. Unsupervised hierarchical clustering analysis confirmed that FLC samples stratify completely separately from NML samples (**Figure 1E**). We then directly compared microRNA profiles between FLC and NML to identify significantly differentially expressed microRNAs (n=23; **Figure 1F**). For each of these microRNAs, we calculated the coefficient of variance (CoV) to measure the level of expression variability across FLC samples. After setting a maximum CoV threshold of 2.0, we identified 20 microRNAs of interest in FLC (11 up-regulated, 9 down-regulated). The expression level of each up- or down-regulated microRNA is shown for each patient (**Figure 1G and H**). The down-regulated set includes miR-375, which we reported previously as a likely tumor suppressor in FLC (22). Due to our previous work on tumor suppressor microRNAs in FLC (22), we focused the remainder of this study on the up-regulated microRNAs, which represent candidate oncogenes. The up-regulated set comprises miR-199b-5p, miR-31-5p, miR-218-1-5p, miR-218-2-5p, miR-203, miR-21-5p+1, miR-708-5p, miR-190b, miR-182-5p, miR-10b-5p, and miR-10b-5p+1 (**Figure 2A**). Among these, miR-10b is the most abundant in FLC tumors (>5-fold more abundant on average than the next-most abundant microRNA).

Within our patient sample set, we have 9 matched samples to compare the microRNA expression in FLC tumor to adjacent NML tissue. The 11 microRNAs up-regulated in the full dataset exhibited very similar expression trends in this matched dataset (**Figure 2B**).

Expression of microRNAs in primary versus metastatic FLC

Next, we analyzed the differential expression of microRNAs in primary or metastatic FLC tumor tissue relative to NML. Primary tumor samples were all hepatic in origin and metastatic samples were from liver, lung, lymph nodes, pancreas, or peritoneum (**Supplemental Table 1**). The expression of microRNAs does not stratify primary from metastatic samples according to PCA (**Figure 3A**). We also observed no specific clustering based on different sites of FLC malignancy (**Figure 3B**), suggesting that FLC maintains highly consistent differential expression of microRNAs irrespective of tumor type or metastatic location. When comparing only primary tumors (n=18) to NML (n=10), we identified 9 up-regulated and 8 down-regulated microRNAs (**Figure 3C, E**). We performed an identical analysis comparing only metastatic tumor tissue (n=19) to NML (n=10) and found that 14 microRNAs are up-regulated and 10 are down-regulated (**Figure 3D, F**). These microRNAs comprise all of those identified in the primary vs. NML analysis (**Figure 3C)** and all-FLC vs. NML analysis (**Figure 1G**), as well as three additional microRNAs, which are isomiRs of miR-21 and miR-203. Upon further analysis of the 14 up-regulated microRNAs, none were found to be significantly differentially expressed in primary versus metastatic FLC tissue (**Supplemental Figure 1**).

Expression of microRNAs in FLC compared to other cancer types

Next, we compared the expression of the 11 up-regulated microRNAs in FLC (9 when discounting isomiRs) (**Figure 1G**) across all 23 cancer types available in The Cancer Genome Atlas (TCGA) for which small RNA sequencing has been performed and non-malignant tissue controls exist. We previously identified (19) 6 FLC samples within TCGA (designated ‘TCGA FLC’), which we report here separately from the set of FLC samples used in this study (designated

'as Cornell/FCF FLC'). We found that only four microRNAs (miR-190b, miR-10b, miR-199b, and miR-218-1) exhibit a level of increased expression in the Cornell/FCF FLC tumors that is greater than the increase observed in any other cancer type (**Figure 4A-D**). We also noted that there are three microRNAs (miR-10b, miR-708, and miR-218-2) which exhibit concordant increases between the Cornell/FCF FLC and TCGA FLC sets, and for which increases in the Cornell/FCF FLC set are most similar to gastrointestinal cancers (in particular colon adenocarcinoma, COAD, and rectal adenocarcinoma, READ) (**Supplemental Figure 2A-E**).

Transcriptional activity at microRNA loci in FLC

Aberrant microRNA expression in cancer can be due to changes in transcriptional and/or post-transcriptional regulation (34). Therefore, we next sought to determine which of the microRNA changes in FLC are driven by transcription. We used our previously published (21) chromatin run-on sequencing (ChRO-seq) data across 13 FLC samples to identify with high-confidence the promotor regions of all microRNAs differentially expressed in FLC (n=20; after removal of isomiRs, n=17) (**Figure 1G, H**). We then used the same ChRO-seq data to quantify the level of transcription from each of the microRNA promoters in FLC vs NML. We observed an overall concordance between the fold-change in transcription (ChRO-seq) and the fold-change in expression (small RNA-seq) for most of the 17 microRNAs (**Figure 5A**). In all cases transcriptional activation or repression led directly to increased or decreased expression, respectively. However, for a few microRNAs, such as miR-203 and miR-378a-5p, the amplitude of the fold-change in expression is much greater than the fold-change in transcription, suggesting that these microRNAs may be altered in FLC primarily by post-transcriptional mechanisms.

MiR-483-5p (**Figure 5B**) and miR-10b (**Figure 5C**) exhibit the greatest decrease and increase in transcription, respectively, in FLC relative to NML (**Figure 5A**). It has been reported in other cancer types (35-37) that miR-10b is transcriptionally activated by the Twist1 transcription factor and we identified a ~3-fold increase of *TWIST1* expression in FLC (**Supplemental Figure 3A**). However, we observed that *TWIST1* is negatively correlated to DP expression (**Supplemental Figure 3B**). We then performed an unbiased search of the miR-10b promoter region using the online resource 'Find Individual Motif Occurrences' (FIMO) (38), which revealed high-confidence binding sites for FOXQ1, as defined by the JASPER transcription factor binding profile database (39). We identified a ~5-fold increase in *FOXQ1* expression in FLC and a significant positive correlation to DP expression (**Supplemental Figure 3C, D**) across 19 FLC samples for which we have matched RNA-seq and small RNA-seq data.

DNAJB1-PRKACA promotes miR-10b expression in human but not mouse cell models

Having identified miR-10b as: (a) one of the most differentially expressed microRNAs in FLC (**Figure 1G**), (b) the most highly expressed among the up-regulated microRNAs in FLC (**Figure 2A**), (c) aberrantly expressed in both primary and metastatic FLC tissue (**Supplemental Figure 1A**), and (d) the most transcriptionally activated microRNA in FLC compared to NML (**Figure 5A**), we next asked if miR-10b is directly responsive to the expression and activity of DP. We constructed lentiviral vectors (21,22) (**Figure 6A**) for transduction and ectopic expression of enhanced green fluorescent protein (GFP), DP, protein kinase A catalytic α subunit (PKA), or a catalytically inactive form of DP carrying a lysine to histidine amino acid substitution at position 128 (K128H). The protein expression of wild type PKA is shown in the GFP samples (lane 1, **Figure 6B; Supplemental Figure 4A, B**) as well as in the three DP-expressing clones (lanes 2-4, **Figure 6B, Supplemental Figure 4A, B**), migrating at approximately 40kD. As expected, there is increased expression of wild-type PKA in the HepG2 line over-expressing PKA (lane 3, **Figure 6B; Supplemental Figure 4A, B**) and DP protein (identified by the higher molecular band migrating at approximately 46kD) is detectable only in the HepG2 lines over-expressing DP or DP-K128H (lanes 2 and 4, **Figure 6B; Supplemental Figure 4A, B**). We observed that the over-expression of DP or wild type PKA leads to a significant increase in the number of metabolically-active, viable cells relative to HepG2-GFP cells (**Figure 6C; Supplemental Figure 4C**), whereas the over-expression of K128H has a much milder impact on the number of viable cells (**Figure 6C; Supplemental Figure 4C**).

Having established that the expression of DP affects cell abundance, we next performed small RNA sequencing in the HepG2-GFP and HepG2-DP cell lines to identify changes in microRNA expression mediated by DP. PCA analysis showed that microRNA profiles stratify replicates of HepG2-GFP from HepG2-DP samples (**Figure 6D**). Differential expression analysis identified 8 microRNAs that are significantly altered in HepG2-DP relative to HepG2-GFP cells (**Figure 6E**). Among these, miR-10b is the most significantly up-regulated (~30-fold). Other microRNAs that we had identified as upregulated in FLC tumors (**Figure 1G**) are not altered by DP in this cell model (**Figure 6E)**. We confirmed by qPCR the dramatic up-regulation of miR-10b in HepG2-DP cells, and showed that miR-10b is not changed in HepG2-

PKA and only modestly changed in HepG2-K128H cells (**Figure 6F**). These data demonstrate that miR-10b increase is specific to DP over-expression. We also analyzed by qPCR the expression of two other microRNAs that are significantly upregulated in FLC, miR-182 and miR-21 (**Figure 1G**), and found that there was no significant induction in the HepG2-DP cell line (**Supplemental Figure 4D**). These data suggest that DP activity has a very robust effect on miR-10b and that the up-regulation of other microRNAs in FLC may be contextual to the unknown cell of origin.

We then turned to another human cell model, HEK293-DP: HEK293 cells in which the ~400kb deletion found in human FLC patients was re-created by CRISPR/Cas9 (40), leading to the expression of DP. We observed by qPCR that miR-10b is significantly elevated (~3-fold) in HEK293-DP cells relative to wild-type HEK293 cells (**Figure 6G**). We next analyzed a single tissue sample from a patient with intraductal oncocytic papillary neoplasm (IOPN) of the pancreas, which is the only other cancer type in which DP has been detected (41) and found that miR-10b is elevated (~1.5 fold) compared to the non-malignant pancreas tissue (**Supplemental Figure 4E**). We also assessed three different murine-based models of FLC: (i) AML-12-DP cells (42), (ii) TIB-75-DP cells (Methods), and (iii) DP-expressing mouse (14) (DP was expressed by *in vivo* transposition). Surprisingly, we found that in all three cases the expression of miR-10b is not increased, and in some cases actually reduced, by the presence of DP (**Supplemental Figure 4F-H**). These findings reveal that DP regulates miR-10b oppositely in human versus mouse cells, and therefore mouse models of FLC are likely not appropriate for studying the role of miR-10b in FLC.

Identification of genes subject to post-transcriptional regulation by microRNAs in FLC

To determine which genes expressed in FLC are likely regulated by microRNAs we performed an integrative analysis of RNA-seq and ChRO-seq data (Methods). We first showed across all genes that the change in transcription is highly correlated with the change in mRNA expression in FLC versus NML (**Figure 7A**), indicating that most gene expression changes in FLC are strongly driven by transcription. Nonetheless, some genes do exhibit robust changes in expression in FLC versus NML despite little-to-no change in transcription, and these are top candidates for post-transcriptional regulation (PTR) by microRNAs. We defined 788 genes that are not significantly changed in FLC according to ChRO-seq signal but are significantly reduced (gain of post-transcriptional regulation, GPR; n=548) or increased (loss of post-transcriptional regulation, LPR; n=240) according to RNA-seq.

To determine whether one or more microRNAs serve as master regulators of the PTR genes, we employed miRhub (43), a bioinformatic tool which determines whether a set of genes is significantly enriched for predicted binding sites of any microRNA. We performed the analysis on GPR (n=548) and LPR (n=240) genes independently. Across both analyses, only two microRNAs emerged as candidate master microRNA regulators: miR-10b for GPR genes (**Figure 7B**) and miR-455 for LPR genes (**Figure 7C**).

Inhibition of miR-10b reduces metabolic activity and proliferation in PDX-derived FLC cell lines

Having determined that miR-10b is a candidate master regulator of GPR genes in FLC, we next sought to evaluate the potential function of miR-10b in FLC. We leveraged a primary human FLC cell line (designated FLC-C) that was established previously from a patient-derived xenograft (PDX) (44) by treating with a locked-nucleic acid (LNA) inhibitor against miR-10b. Following transfection, we assessed the impact on cell health and proliferation. We found that the number of metabolically-active, viable cells is significantly reduced after miR-10b inhibition (**Supplemental Figure 5A, B**).

There are several limitations of the FLC-C line (21), including that it is viable for only very few passages; therefore, we pursued analysis of miR-10b function in an independently PDX-derived human FLC cell line (designated FLC-H). DP protein expression in FLC-H cells is similar to that of primary FLC tumors (**Figure 8A; Supplemental Figure 4A, B**). The FLC-H cell line, and the PDX tumor from which it was derived, express both the major and minor isoform of DP, whereas the FLC tumor control used only expresses the major form of DP (10). We analyzed the expression of miR-10b by qPCR in FLC-H cells – although levels are slightly lower than in FLC tumor samples (**Supplemental Figure 5C**), they are highly stable across multiple passages (**Supplemental Figure 5D**). With this improved cell line, we confirmed that miR-10b abundance is dramatically reduced after transfection with the LNA inhibitor (**Figure 8B**). We then confirmed that miR-10b reduction leads to modest (~25%) but significant reduction in metabolically-active, viable cells as measured by CellTiter-Glo (n=6 independent experiments representing 34 biological replicates, **Figure 8C**).

Predicted targets of miR-10b among the GPR genes include Fanconi Anemia Complement Group C (*FANCC*), Kruppel Like Factor 11 (*KLF11*), SEC14 Like Lipid Binding 2 (*SEC14L2*), Sirtuin 5 (*SIRT5*), Sad1 and UNC84 Domain Containing 2 (*SUN2*), and Tripartite Motif Containing 35 (*TRIM35*), all of which have been implicated previously in the control of cell proliferation (25,28,31,45-48). We measured the expression level of these genes by qPCR after LNA-mediated miR-10b inhibition and observed small but significant changes in *KLF11, SIRT5,* and *SEC14L2*, a modest and significant up-regulation of *FANCC and SUN2*, and a robust and significant increase in expression of *TRIM35* (~2-fold) (**Figure 8D**). We then measured the expression of these genes after transfection of a miR-10b mimic (MIM), which dramatically increased the abundance of miR-10b (**Supplemental Figure 5E**). We first measured previously reported targets of miR-10b (37), *CDH1* and *PTEN*, and found that neither LNA-10b nor MIM-10b altered the expression of these genes (**Supplemental Figure 5F**). We did, however, observe a modest reduction of *SIRT5*, *SUN2*, and *TRIM35*, and a significant reduction of *FANCC* mRNA after MIM-10b treatment (**Supplemental Figure 5G**). Based on the known functions of FANCC, TRIM35, and SUN2, we hypothesized that the reduction in viable cells after miR-10b inhibition is due to reduced proliferation. To test this, we performed an anchorage-independent growth assay, an EdU incorporation assay (to assess replication and synthesis), and also carried out TUNEL staining (to assess apoptotic induction) in the FLC-H cell line. Inhibition of miR-10b leads to a significant reduction in colony growth (~40%) (**Figure 8E, F**) and EdU incorporation (~25%) (**Figure 8G, H**), but no change in TUNEL staining (**Supplemental Figure 5H, I**). Taken together, these results indicate that miR-10b regulates cell proliferation but not apoptosis in FLC cells.

Discussion

FLC is an aggressive cancer afflicting young adults who lack underlying predisposition to liver cancer. Surgical resection is the primary remedy for FLC, but advanced disease is incurable as there are no standard-of-care therapeutics. While it is well established that patients with FLC harbor the novel oncogene *DNAJB1-PRKACA* (DP), a direct and specific inhibitor of the DP enzyme is unavailable. Furthermore, it remains unclear whether DP is essential for tumor progression, maintenance, and metastasis. For these reasons, there is a dire need to identify alternative therapeutic strategies. Toward that end, it is important first to deepen understanding of the molecular underpinnings of FLC etiology and progression. In this study, we focused our investigation on the contributions of post-transcriptional gene regulation and microRNA activity toward shaping gene expression profiles and tumor phenotypes of FLC.

We first performed microRNA analysis in the largest FLC and NML sample set to date – more than three times as large as our previous study, which centered on the potential role of miR-375 as a tumor suppressor in FLC (22). The sample set used in the present study enabled analyses that were infeasible in previous studies of microRNAs in FLC (22,23). Specifically, we were able to compare matched samples from the same patient and also directly compare primary vs. metastatic FLC. Moreover, we were also able to assess the potential effect of metastatic location on the microRNA landscape.

A major novelty and strength of the study is the inclusion of ChRO-seq data to quantify the rates of transcription for microRNAs that we found to be differentially expressed in FLC. In most cases, the change in transcription at a microRNA locus (as determined by ChRO-seq) matches the change in expression of the mature microRNA (as determined by small RNA-seq). However, there were some notable exceptions, such as miR-203 and miR-378a-5p. For these microRNAs, the amplitude of the fold-change in expression is much greater than the fold-change in transcription, suggesting that they may be altered in FLC primarily by post-transcriptional mechanisms.

Another new aspect of the current study is the integrative analysis of ChRO-seq and RNA-seq data to identify a high-confidence list of genes that are subject primarily to post-transcriptional regulation in FLC. Specifically, we defined those genes that change significantly in expression in FLC due primarily to gain of post-transcriptional regulation (GPR) or loss of post-transcriptional regulation (LPR). GPR and LPR genes represent the top candidate targets of microRNAs and RNA binding proteins (RBPs), which are the major mechanisms of post-transcriptional gene expression control. In this study, we focused on microRNAs, but the contribution of RBPs merits investigation in the future. We found that miR-10b is the top candidate master regulator of GPR genes and miR-455-3p is the top candidate master regulator of LPR genes.

Although we found that several microRNAs are altered in FLC, we decided to pursue miR-10b for functional studies for three major reasons brought to light by our study: (a) it is the most highly expressed among the up-regulated microRNAs in FLC; (b) it is the most transcriptionally activated microRNA in FLC compared to NML; and (c) it is the only up-regulated microRNA in FLC that is specifically and robustly responsive to DP activity (and not just wild-type PKA activity) in two different human cell models (HepG2 and HEK293). Interestingly, miR-10b levels are not increased by the

presence of DP in two different mouse cell models or the only available *in vivo* mouse model, which suggests that the regulatory connection between DP and miR-10b is species-specific. It is important to note here the limitation that HepG2 and HEK293 cell models do not replicate the environment in which FLC tumors are initiated in humans, though the data from the analysis of the tissue from the patient with IOPN does provide *in vivo* support for a regulatory connection between DP and miR-10b. The FLC cell-of-origin has not yet been determined, though at least one study has suggested biliary tree stem cells as a possibility (44). In the future, it will be important to assess whether miR-10b and other FLC markers and candidate drivers are sensitive to DP activity in biliary tree stem cells or other candidate cells-of-origin.

In other cancer types the transcription factor TWIST1 promotes miR-10b expression (49,50), and the activation of TWIST1 protein by phosphorylation is PKA dependent (51,52). Considering that DP is a chimera that maintains PKA catalytic activity, a similar mechanism may operate in FLC. TWIST1 activity is also enhanced by the transcription factor FOXQ1 (53) and we predicted several high-confidence FOXQ1 binding sites in the promoter of miR-10b in FLC. FOXQ1 promotes PI3K/AKT activity in colorectal cancer (54) and the abundant expression of FOXQ1 in FLC suggests that a similar mechanism may exist. The potential role of FOXQ1 in promoting miR-10b expression in FLC, with or without TWIST1, is intriguing and merits further investigation. MiR-10b has been shown to contribute to the progression of 15 different cancer types (37), generally by promoting cancer cell metastasis. In our experiments, we found that the up-regulation of miR-10b in FLC is greater than in any other cancer type for which data is available in TCGA. Our finding that *TRIM35* is regulated by miR-10b is novel. In hepatocellular carcinoma, TRIM35 has been identified as a tumor suppressor (31) by limiting the stability of pyruvate kinase and reducing cellular energetics. In future studies, it will be interesting to evaluate whether miR-10b controls glycolysis in FLC cells and whether this regulation is mediated by suppression of TRIM35. MiR-10b regulation of SUN2 is also new. The reported role of SUN2 in suppressing the Warburg effect (25) provides another clue about the potential role of miR-10b in promoting glycolysis in FLC cells.

The functional experiments in this study revealed that suppression of miR-10b in FLC cells leads to a modest but significant reduction in metabolic activity, anchorage-independent cell growth, and proliferation. These results point to a role for miR-10b in promoting the growth of FLC cells. Due to the modest effects of miR-10b on growth/proliferation, we do not propose that a miR-10b inhibitor is by itself a candidate therapeutic modality. However, we do believe that the functions of miR-10b in FLC are worth studying further in improved models of FLC (e.g., additional PDX models or direct patient-derived cells) and that in the future it may be worth considering a miR-10b inhibitor as part of a combinatorial therapeutic approach. Interestingly, many genes established as miR-10b targets previously in other cancer types, such as *PTEN* (55), were not identified as significantly altered in FLC, which speaks to the growing appreciation for contextual assessment of microRNA targets. Also, although we did not functionally interrogate miR-455-3p in this study, we believe it merits consideration in the future, especially since it has been reported already as a key suppressor of invasion and metastasis in other aggressive cancers, particularly esophageal squamous cell carcinoma, colorectal cancer, breast cancer, melanoma, and pancreatic cancer (56-59).

Materials and Methods

Human Samples

Informed consent was obtained from all individuals. Tumor and adjacent non-malignant liver samples were collected from patients with FLC by surgeons and provided by the Fibrolamellar Cancer Foundation. Patients included male and female subjects and some samples were collected from the same patient. All samples were de-identified before shipment to Cornell. Additional sample information is detailed in Supplemental Table 1.

The tissue sample from the patient with intraductal oncocytic papillary neoplasm, as well as the adjacent normal pancreas tissue sample, was obtained from Dr. Olca Basturk at the Memorial Sloan Kettering Cancer Center (New York, New York).

Animal Samples

Liver samples from female C57BL/6N mice on 3,5-diethoxycarbonyl-1,4-dihydrocollidine (DDC, 0.1%) diet were obtained from a previous study(14). These liver samples expressed human *DNAJB1-PRKACA*, beta-catenin, both DNAJB1-PRKACA and beta-catenin, or an empty vector control and were collected 4.5 months after transposition of *DNAJB1-PRKACA.*

Cell lines

HepG2 cells obtained from the American Type Culture Collection (ATCC; Manassas, VA). HepG2 cells expressing *GFP*, *DNAJB1-PRKACA*, *PRKACA*, or the *DNAJB1-PRKACA* K128H mutant have been previously described (21,22). HepG2 cells were cultured in Dulbecco's Modified Eagle Media (DMEM) containing 1g/L glucose (Thermo Fisher Scientific) supplemented with 10% fetal bovine serum (Thermo Fisher Scientific), 1% GlutaMAX (Thermo Fisher Scientific), 110mg/L sodium pyruvate (Thermo Fisher Scientific), 1% penicillin-streptomycin (Thermo Fisher Scientific), and puromycin 5 ug/mL (Thermo Fisher Scientific).

AML-12 cells expressing *DNAJB1-PRKACA* have been previously described (42) and were grown in DMEM:F12 medium (Thermo Fisher Scientific) supplemented with 10% fetal bovine serum (Thermo Fisher Scientific), 10ug/mL insulin (Thermo Fisher Scientific), 5.5 ug/mL transferrin (Thermo Fisher Scientific), 5 ng/mL selenium (Thermo Fisher Scientific), and 40ng/mL dexamethasone (Thermo Fisher Scientific).

HEK293 cells expressing *DNAJB1-PRKACA* have been previously described (40) and were grown in in Dulbecco's Modified Eagle Media (DMEM) containing 4.5g/L glucose (Thermo Fisher Scientific) supplemented with 10% fetal bovine serum (Thermo Fisher Scientific), 1% GlutaMAX (Thermo Fisher Scientific), 110mg/L sodium pyruvate (Thermo Fisher Scientific), 1% penicillin-streptomycin (Thermo Fisher Scientific).

TIB75 cells expressing *DNAJB1-PRKACA* were obtained as a gift from Dr. Mark Yarchoan (Johns Hopkins, Baltimore, MD). TIB75 cells are derived from embryonic murine liver epithelia then transformed with methylcholanthrene epoxide and made available through the American Type Culture Collection (ATCC). Cells were treated with a CRISPR/Cas9 guide and selected as previously described (42). These cells were grown in in Dulbecco's Modified Eagle Media (DMEM) containing 4.5g/L glucose (Thermo Fisher Scientific) supplemented with 10% fetal bovine serum (Thermo Fisher Scientific), 1% GlutaMAX (Thermo Fisher Scientific), 110mg/L sodium pyruvate (Thermo Fisher Scientific), 1% penicillin-streptomycin (Thermo Fisher Scientific).

FLC-C cells were generated from a patient-derived xenograft model (44) and grown in advanced DMEM media conditioned by irradiated mouse embryonic fibroblasts containing 300mg/L l-glutamine (Thermo Fisher Scientific) supplemented with 10% fetal bovine serum (Thermo Fisher Scientific), 1% penicillin-streptomycin (Thermo Fisher Scientific). The media was supplemented with 10% DMEM conditioned by R-spondin secreting human embryonic kidney cells and 20uM Y-27632 ROCK inhibitor as previously described (21).

FLC-H cells were generated from a patient-derived xenograft model (44) and grown in RPMI1640 media containing 300mg/L l-glutamine (Thermo Fisher Scientific) supplemented with 10% fetal bovine serum (Thermo Fisher Scientific),

1% penicillin-streptomycin (Thermo Fisher Scientific) and 2.5 ug/mL human hepatic growth factor (Thermo Fisher Scientific).

All cell lines were cultured in a humid chamber at 37°C and 5% CO2.

Small RNA library preparation and sequencing

Frozen tumors underwent physical dissociation using a polytron PT1200 E homogenizer (Thomas Scientific, Swedesboro, NJ) and total RNA was isolated with the Total RNA Purification Kit (Norgen Biotek) as per the manufacturer's instructions. RNA purity was quantified with the Nanodrop 2000 instrument (Thermo Fisher Scientific, Waltham, MA) and RNA integrity was quantified with the Agilent 4200 Tapestation (Aglient Technologies, Santa Clara, CA). Libraries were generated using the CleanTag Small RNA Library Prep Kit (TriLink Biotechnologies, San Diego, CA). Sequencing was performed on the HiSeq2000 or HiSeq3000 platforms (Illumina, San Diego, CA) at the Genome Sequencing Facility of the Greehey Children's Cancer Research Institute (University of Texas Health Science Center, San Antonio, TX). RNA from cell lines was purified and sequenced as described above except without polytron homogenization.

PolyA+ RNA library preparation and sequencing

Of the 27 RNA-seq datasets analyzed in this study, 18 were generated and published previously (21), and 9 were newly generated. For the newly generated data, total RNA was isolated using the Total RNA Purification Kit (Norgen Biotek) per manufacturer's instructions. RNA purity was quantified with the Nanodrop 2000 (Thermo Fisher Scientific, Waltham, MA) or Nanodrop One and RNA integrity was quantified with the Agilent 4200 Tapestation (Agilent Technologies, Santa Clara, CA). Libraries were prepared by the Cornell Transcriptional Regulation and Expression (TREx) Facility using the NEBNext Ultra II Directional RNA kit. Sequencing was performed at the Biotechnology Research Center at Cornell University on the NextSeq500 (Illumina).

Chromatin run-on library preparation and sequencing

All ChRO-seq datasets (n=13) analyzed in this study were generated and published previously (21).

Bioinformatic analysis

Small RNA sequencing was processed using miRquant 2.0 as previously described (33). In brief, miRquant 2.0 trims the 3' adapter from small RNA reads, aligns reads to the genome (hg19), annotates miRNAs (miRbase v18), identifies deviations from canonical miRNAs (iso-miRNAs, non-template additions, internal edits), and quantifies aligned reads as both raw counts and normalized reads per million mapped to miRNAs (RPMMM). Raw counts were analyzed using DESeq2.0 (v1.3) to obtain normalized counts and determine differential expression, using a model that includes sequencing batch as a covariate. For visualization and clustering, normalized counts were transformed using a variance stabilizing transformation and corrected for batch effect using the removeBatchEffect function from the limma package. Normalized small RNA sequencing data available from The Cancer Genome Atlas (TCGA) was acquired using TCGA-assembler 2 and comparative analysis was performed as previously described (22).

Paired end RNA sequencing reads were aligned to the human genome (hg38) using STAR (v2.4.2a) and reads aligning to the transcriptome were quantified using Salmon (v0.6). Differential expression was determined with DESeq2.0 (v1.3) using a model that accounts for sequencing facility as a covariate.

miRhub (43) was used to determine if putative microRNA binding sites are enriched in a list of differentially expressed genes. In brief, miRhub uses a gene list, usually up or down regulated genes, as an input. For each microRNA, the cumulative number of putative microRNA binding sites in the 3' UTR of those genes represents the score for that microRNA. Using a Monte-Carlo simulation, this process is repeated 1000 times using random gene lists of the same length. The score from the input gene list is compared to scores of the simulated gene lists to determine significance.

Quantification of transcriptional activity at microRNA loci

Chromatin run-on sequencing (ChRO-seq) data was published previously (21). MicroRNA loci were defined as the beginning of the nearest upstream transcriptional regulatory element (TRE), defined as the promoter, to the end of the mature microRNA. Total ChRO-seq signal was calculated in this region as a measure of transcriptional activity. Genomic loci snapshots were generated using Gviz 1.26.5
.

Integration of RNA-seq and ChRO-seq data to identify genes subject primarily to post-transcriptional regulation

We first performed a differential transcription analysis of gene bodies and differential expression analysis of genes independently using the DESeq2.0 (v1.3). Genes gaining post-transcriptional regulation were identified as those not altered at the transcriptional level between FLC and NML (ChRO-seq log2FC > -0.59 and ChRO-seq FDR > 0.2), but significantly down-regulated at the steady state gene expression level (RNA-seq average NML counts > 1000, RNA-seq log2FC < -1, and RNAseq FDR < 0.05). Genes losing post-transcriptional regulation were identified as those not altered at the transcriptional level between FLC and NML (ChRO-seq log2FC < 0.59 and ChRO-seq FDR > 0.2), but significantly up-regulated at the steady state gene expression level (RNA-seq average FLC counts > 1000, RNA-seq log2FC > 1, and RNA-seq FDR < 0.05). We determined using miRhub if predicted targets of any of the FLC-dysregulated microRNAs were significantly enriched in these lists of post-transcriptionally regulated genes.

Quantitative PCR

Total RNA was isolated from tissue or cells using Total RNA Purification Kit (Norgen Biotek) as per manufacturer's instructions. Reverse Transcription was performed using the High-Capacity RNA-to-cDNA Kit (Thermo Fisher Scientific) for gene analysis or using the TaqMan MircoRNA Reverse Transcription Kit (Thermo Fisher Scientific) for microRNA analysis. Gene and microRNA expression were quantified with TaqMan Expression assays on a CFX96 Touch Real-Time System thermocycler (Bio-Rad). Gene expression assays were normalized to the expression of *RPS9* and microRNA expression assays were normalized to the expression of *RNU6*. Individual gene assay IDs: CDH1, hs01023895; DNAJB1-PRKACA, custom; FANCC, hs0098454; KLF11, hs00231614; miR-10b, 002218, miR-21, 000397; miR-182, 002334; PTEN, hs02621230; RNU6, 001973; RPS9, hs02339424; SEC14L2, hs00391446; SIRT5, hs00978331; SUN2, hs00391446; TRIM35, hs00324633 (Thermo Fisher Scientific). Expression values reported are averaged across at least three biological replicates unless otherwise stated in the main text.

Immunoblot analysis

HepG2 and FLC-H cells were lysed in RIPA buffer containing Halt protease and phosphatase inhibitors (Thermo Fisher Scientific) at 4°C. Cells were incubated for 30 minutes and centrifuged at 14,000 X g for 10 minutes at 4°C. Total protein in the supernatant was quantified using the BCA Protein Assay Kit (Thermo Fisher Scientific). Samples were denatured in NuPAGE LDS Sample Buffer (Thermo Fisher Scientific) containing 5% β-Mercaptoethanol for 10 minutes at 70°C and loaded to a 12% SDS-polyacrylamide gel. After electrophoresis, samples were transferred to polyvinylidene difluoride membrane and blocked in Tris buffered saline containing 0.5% TWEEN20 (TBST) and 3% bovine serum albumin for 1 hour at room temperature. Membranes were probed for anti-PRKACA (1:1000 dilution, rabbit source, Cell Signaling 4782) or anti-Vinculin (1:1000 dilution, Invitrogen MA5-11690) overnight at 4°C and then incubated with goat anti-rabbit HRP linked IgG (1:10000, Cell signaling). Membranes were visualized using a ChemiDoc MP (Bio-Rad).

Cell count, alamar Blue, Cell Titer Glo, EdU incorporation, soft agar, and TUNEL assays

HepG2 cell lines were plated at a density of 10,000 cells/ well in 6-well plates. Cells were collected daily for five days, stained with trypan blue, counted with a TC20 automated cell counter (Bio-Rad). Six independent counts were performed, and the assay was repeated twice.

FLC-H cells were plated at a density of 10,000 cells/ well in 96-well plates. After overnight incubation, cells were transfected with miR-10b LNA inhibitor or scramble negative control (Qiagen) at a 500nmol/L final concentration using Lipofectamine 3000 (Thermo Fisher Scientific) according to manufacturer’s instructions. Six days post-transfection cells were assayed for health using Alamar Blue or the Cell Titer Glo Kit (Promega). To determine the metabolic health of cells, Alamar Blue was added to cells as per the manufacturer’s instruction, incubated for 3 hours, and assayed for spectral absorbance at 570nm. The Cell Titer Glo assay was used to determine the amount of ATP as Relative Fluorescent Units (RFU) of luciferase activity. For each experiment, the signal across six wells was averaged and normalized to the scramble LNA treated cells.

To quantify anchorage-independent growth, FLC-H cells were plated at a density of 10,000 cells/well in 6-well plates. Cells are mixed with media containing 0.3% agar and plated on a pre-hardened layer of media containing 0.6% agar. Both layers of media contain LNA at a concentration of 500nmol/L. Cells were incubated for 35 days and provided supplemental media containing 0.3% agar and LNA to prevent drying. At the end of the growth period, 200uL of a 1mg/ml solution of nitro blue tetrazolium chloride was added to each well and incubated overnight at 37°C. Eight biological replicates were performed and at least ten independent fields per well were imaged. Images were manually analyzed in ImageJ (National Institutes of Health, Bethesda, MD) and data is represented as the percent area stained.

To quantify the proliferation rate, six days post-transfection the cells were treated for 2 hours with 10µmol/L EdU. EdU labeled cells were washed with phosphate-buffered saline, fixed in 4% paraformaldehyde for 20 minutes, and permeabilized with 0.5% Triton-x 100 for 20 minutes. EdU was detected using the Click-iT Plus EdU Alexa Fluor 594 Imaging kit (Thermo Fisher Scientific) according to the manufacturer's instructions with reaction volumes appropriately scaled for 96-well plates.

To quantify apoptosis, six days post-transfection the cells were washed with phosphate-buffered saline, fixed in 4% paraformaldehyde for 20 minutes, and permeabilized with 0.5% Triton-x 100 for 20 minutes. Apoptotic cells were detected using the Click-iT TUNEL Alexa Fluor 488 Imaging kit (Thermo Fisher Scientific) according to the manufacturer's instructions with reaction volumes appropriately scaled for 96-well plates.

After EdU and TUNEL detection, the cells were counterstained with DAPI. Images were collected on a ZOE Fluorescent Cell Imager (Bio-Rad). For each experiment four independent fields per well were imaged. Images were manually analyzed in ImageJ. EdU and TUNEL positive cells are represented as a ratio of all cells in each field, which was averaged and normalized to the scramble treated cells. Each assay was performed with 6 biological replicates unless otherwise stated in the text.

Statistical analysis

Statistical comparisons of quantitative PCR, Alamar Blue, Cell Titer Glo, EdU, and TUNEL results were made using Student's t-test. False discovery rate was controlled for by applying Benjamini-Hochberg correction to experiments where multiple comparisons were made. Significant differences in gene expression or transcriptional signal were determined using DESeq2.0. Graphs were generated in the R software package and error bars represent the standard error.

Data availability

All unpublished small RNA-seq and RNA-seq data can be downloaded from Gene Expression Omnibus (GEO) using the following GEO accession number: GSE181922. Previously published small RNA-seq can be downloaded from GEO using GEO accession number: GSE114974. Previously published RNA-seq and ChRO-seq can be downloaded from the European Genome-Phenome Archive (EGA) using the following EGA accession number: EGAS00001004169.

Study Approval

Informed consent was obtained from all individuals involved in this study and approved by the Institutional Review Board protocols 1802007780, 1811008421 (Cornell University) and 33970/1 (Fibrolamellar Cancer Foundation). Animal samples used in this study were supplied by Dr. Scott Lowe at the Memorial Sloan Kettering Cancer Center (New York, New York) and approved by the Institutional Animal Care and Use Committee protocol 11-06-011 (the Memorial Sloan Kettering Cancer Center).

Author Contributions

ABF designed the study; acquired, analyzed, and interpreted data; prepared figures; provided statistical analysis; and drafted the manuscript. MK analyzed and interpreted data; prepared figures; provided statistical analysis; and edited the manuscript. APM acquired, analyzed, and interpreted data; and edited the manuscript. TAD and RS provided material support and edited the manuscript. KV and NB obtained funding and provided resources. PS designed the study; analyzed and interpreted data; drafted the manuscript; obtained funding; and supervised the study.

Acknowledgements

We would like to thank Dr. Olca Basturk from the Memorial Sloan Kettering Cancer Center for providing the intraductal oncocytic pancreatic neoplasm (IOPN) sample, Dr. Mark Yarchoan from the Liver Cancer Multidisciplinary Clinic of the Johns Hopkins School of Medicine for providing the TIB-75 cells, and Zhao Lai from the Genome Sequencing Facility of the Greehey Children's Cancer Research Institute of the University of Texas Health Science Center at San Antonio for assistance with small RNA sequencing. We would also like to thank Dr. Mark Furth, John Hopper, Marna Davis, Dr. Patricia Cogswell, and the entire Fibrolamellar Cancer Foundation (FCF) for their generous funding, their tireless efforts to support FLC patients, and their maintenance of the FCF tissue biobank. Finally, we are grateful for all of the members of the Sethupathy lab, especially Donald Long, Rosanna Ma, Alaa Farghli, and Rebecca Cubitt for their valuable feedback and intellectual support. Schematics were designed in BioRender.

Figure 1

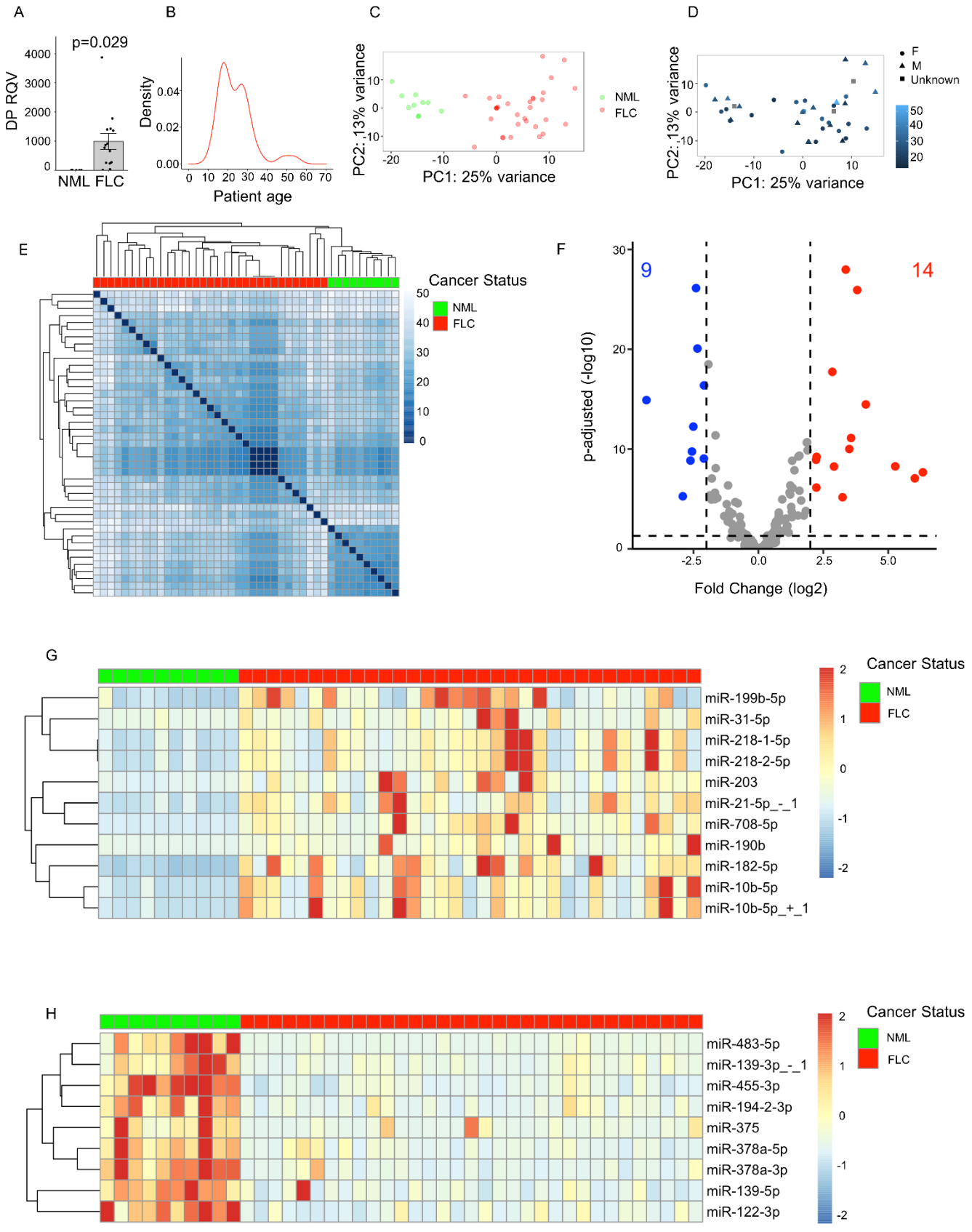
A
p=0.029
DP RQV
NML FLC
B
Density
Patient age
C
PC2: 13% variance
PC1: 25% variance
NML
FLC
D
PC2: 13% variance
PC1: 25% variance
F
M
Unknown
E
Cancer Status
NML
FLC
F
9
14
p-adjusted (-log10)
Fold Change (log2)
G
Cancer Status
NML
FLC
miR-199b-5p
miR-31-5p
miR-218-1-5p
miR-218-2-5p
miR-203
miR-21-5p_-_1
miR-708-5p
miR-190b
miR-182-5p
miR-10b-5p
miR-10b-5p_+_1
H
Cancer Status
NML
FLC
miR-483-5p
miR-139-3p_-_1
miR-455-3p
miR-194-2-3p
miR-375
miR-378a-5p
miR-378a-3p
miR-139-5p
miR-122-3p

Figure 1. miR-10b is among the most upregulated microRNAs in FLC. (A) Quantitative PCR showing the RQV of DP in a subset of FLC samples (n=15) compared to NML samples (n=6). Data points represent individual patient samples. Cycle threshold values can be found in Table 1. **(B)** Patient age distribution across FLC samples used in this study for which age is known (n=35). **(C)** Principal component analysis of VST normalized counts for the NML (n=10) and FLC (n=33) dataset. The percent of variation explained is indicated for component 1 (x-axis) and component 2 (y-axis). NML and FLC samples are colored green and red. **(D)** Principal component analysis plot in which the patient age and gender information are overlayed. Female, male, and unreported patients are indicated by circles, triangles, and squares. The color intensity, from dark to light, indicates increasing patient age at the time of surgery. **(E)** Unsupervised hierarchical clustering of the Euclidean distances among samples was calculated based on VST normalized counts. FLC and NML samples are indicted by red and green boxes. **(F)** Volcano plot showing microRNAs that are significantly differentially expressed (average normalized counts > 1000 in either NML or FLC, coefficient of variance < 2 across FLC samples). Dashed lines represent the log2 FC of expression -2/+2 (vertical) and adjusted $P = 0.05$ (horizontal). Up- or down-regulated microRNAs are colored red or blue, respectively. **(G,H)** Heatmaps showing the normalized expression of up- or down-regulated microRNAs (in rows) in each patient sample (in columns). Expression is scaled by row with a max/min of 2/-2 shown. *P*-values are calculated by two-tailed Student's t-test

Figure 2

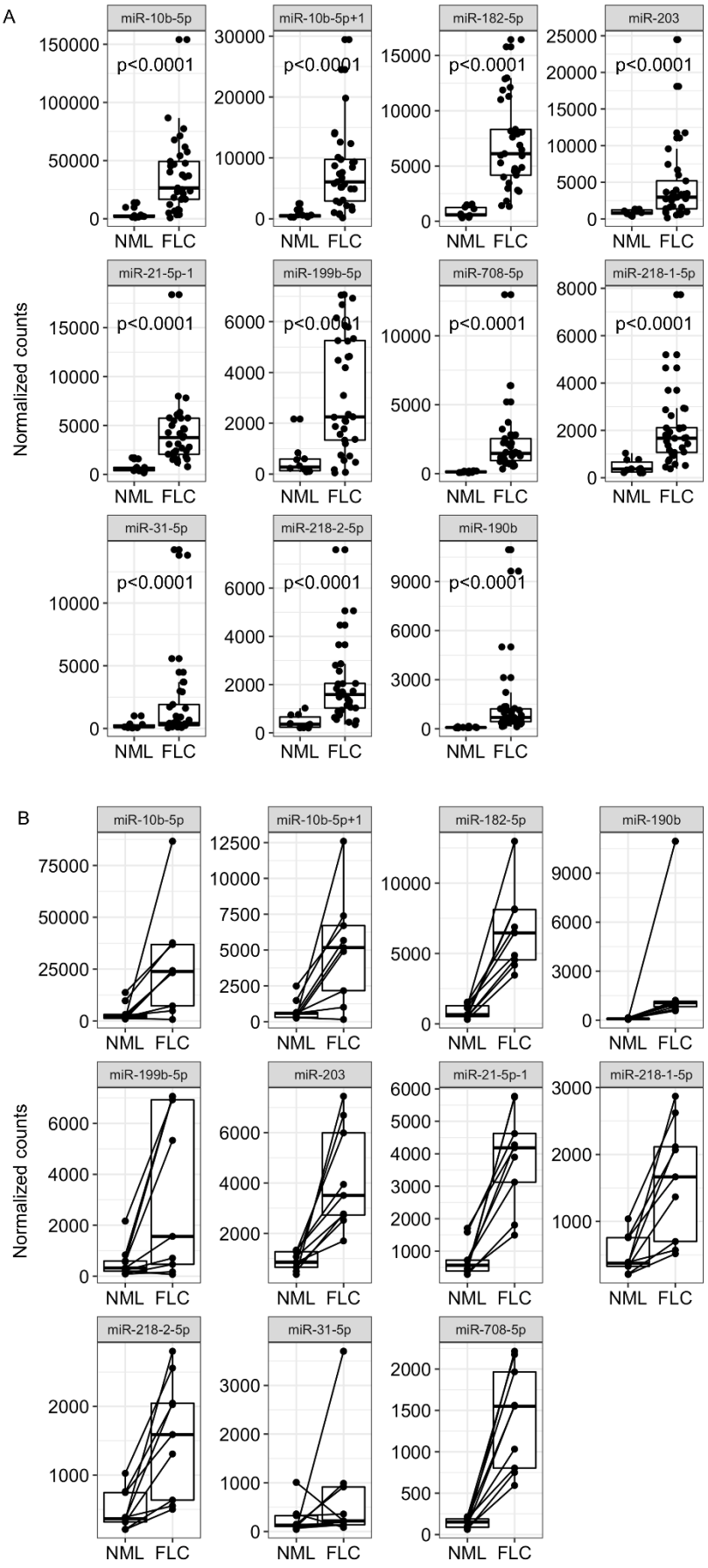
A
B
Normalized counts
miR-10b-5p
miR-10b-5p+1
miR-182-5p
miR-203
miR-21-5p-1
miR-199b-5p
miR-708-5p
miR-218-1-5p
miR-31-5p
miR-218-2-5p
miR-190b
p<0.0001
NML
FLC

Figure 2. Expression levels of the significantly up-regulated microRNAs in all FLC patient samples. (A) The normalized expression of each up-regulated microRNA is shown as individual box plots for NML and FLC. Samples are plotted as individual points. **(B)** Expression of up-regulated microRNAs among FLC patients with matched NML samples (n=9). The matched NML/FLC samples are indicated with a line linking the two data points. Each data point represents a patient sample. *P*-values are calculated by two-tailed Student's t-test.

Figure 3

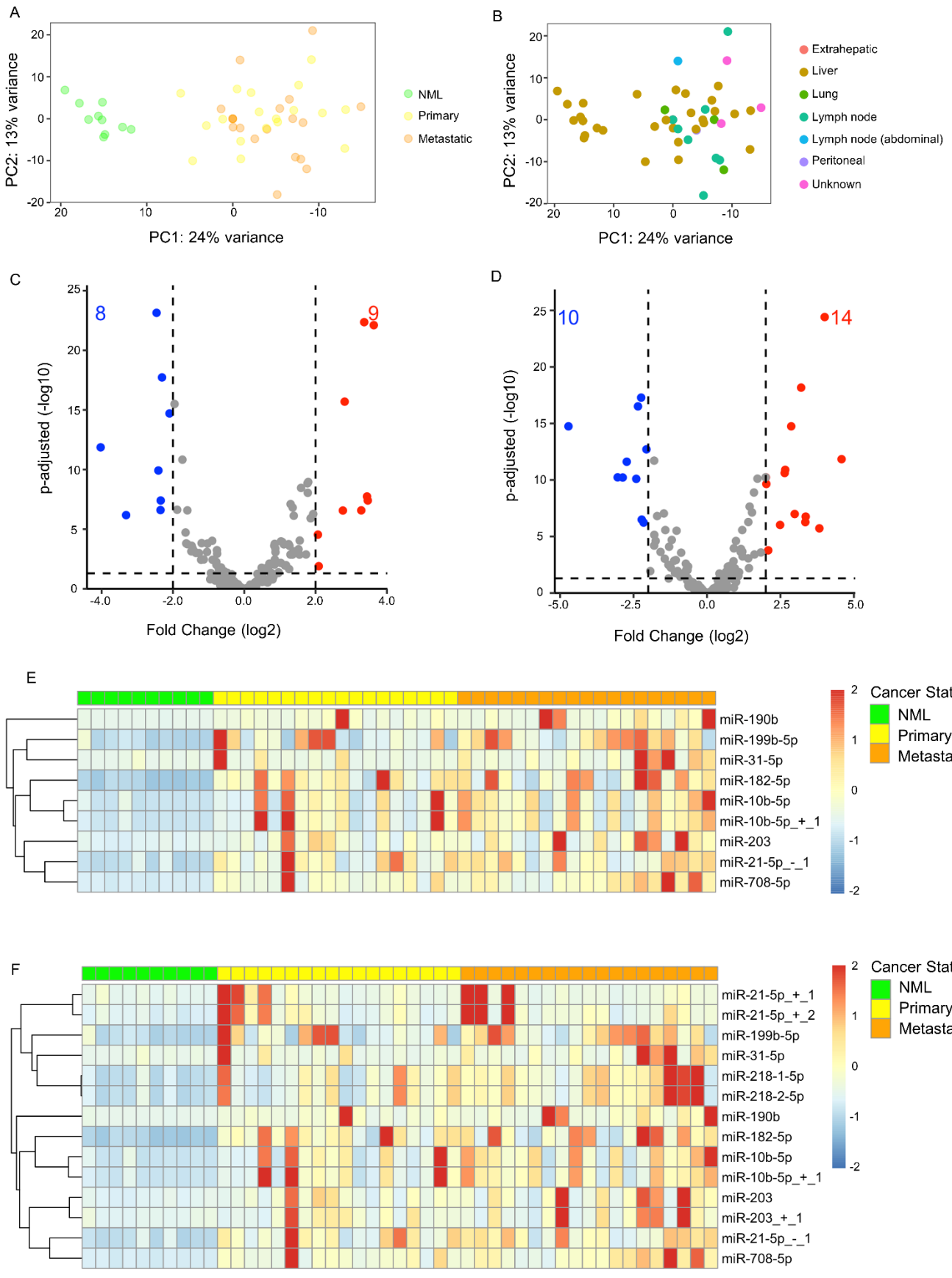
A
PC2: 13% variance
PC1: 24% variance
NML
Primary
Metastatic
B
PC2: 13% variance
PC1: 24% variance
Extrahepatic
Liver
Lung
Lymph node
Lymph node (abdominal)
Peritoneal
Unknown
C
8
9
p-adjusted (-log10)
Fold Change (log2)
D
10
14
p-adjusted (-log10)
Fold Change (log2)
E
miR-190b
miR-199b-5p
miR-31-5p
miR-182-5p
miR-10b-5p
miR-10b-5p_+_1
miR-203
miR-21-5p_-_1
miR-708-5p
Cancer Status
NML
Primary
Metastatic
F
miR-21-5p_+_1
miR-21-5p_+_2
miR-199b-5p
miR-31-5p
miR-218-1-5p
miR-218-2-5p
miR-190b
miR-182-5p
miR-10b-5p
miR-10b-5p_+_1
miR-203
miR-203_+_1
miR-21-5p_-_1
miR-708-5p
Cancer Status
NML
Primary
Metastatic

Figure 3. miR-10b is among the most upregulated microRNAs in both primary and metastatic FLC. (A) Principal component analysis of VST normalized counts with tumor type information overlayed. NML (n=10), primary (n=18), and metastatic (n=19) samples are shown in green, yellow, and orange. **(B)** Principal component analysis of VST normalized counts with metastatic location information overlayed. Extrahepatic, liver, lung, lymph node, peritoneal, and unknown locations are shown red, brown, green, teal, blue, and purple. **(C)** Volcano plot showing microRNAs that are significantly differentially expressed in primary FLC vs. NML (average normalized counts > 1000 in either NML or primary FLC). Dashed lines represent the log2 FC of expression -2/+2 (vertical) and adjusted *P*=0.05 (horizontal). Up- or down-regulated microRNAs are colored red or blue. **(D)** Volcano plot showing microRNAs that are significantly differentially expressed in metastatic FLC vs. NML (analysis criteria identical to panel C). Dashed lines represent the log2 FC of expression -2/+2 (vertical) and adjusted *P*=0.05 (horizontal). Up- or down-regulated microRNAs are colored red or blue. **(E)**. Heatmap showing the expression of microRNAs up-regulated in primary FLC vs. NML. MicroRNAs are listed in rows and individual patients are listed in columns. Expression is scaled by row with a max/min of 2/-2 shown. **(F)** Heatmap showing the expression of up-regulated microRNAs in metastatic FLC vs. NML (sample arrangement is identical to panel E). Expression is scaled by row with a max/min of 2/-2 shown.

Figure 4

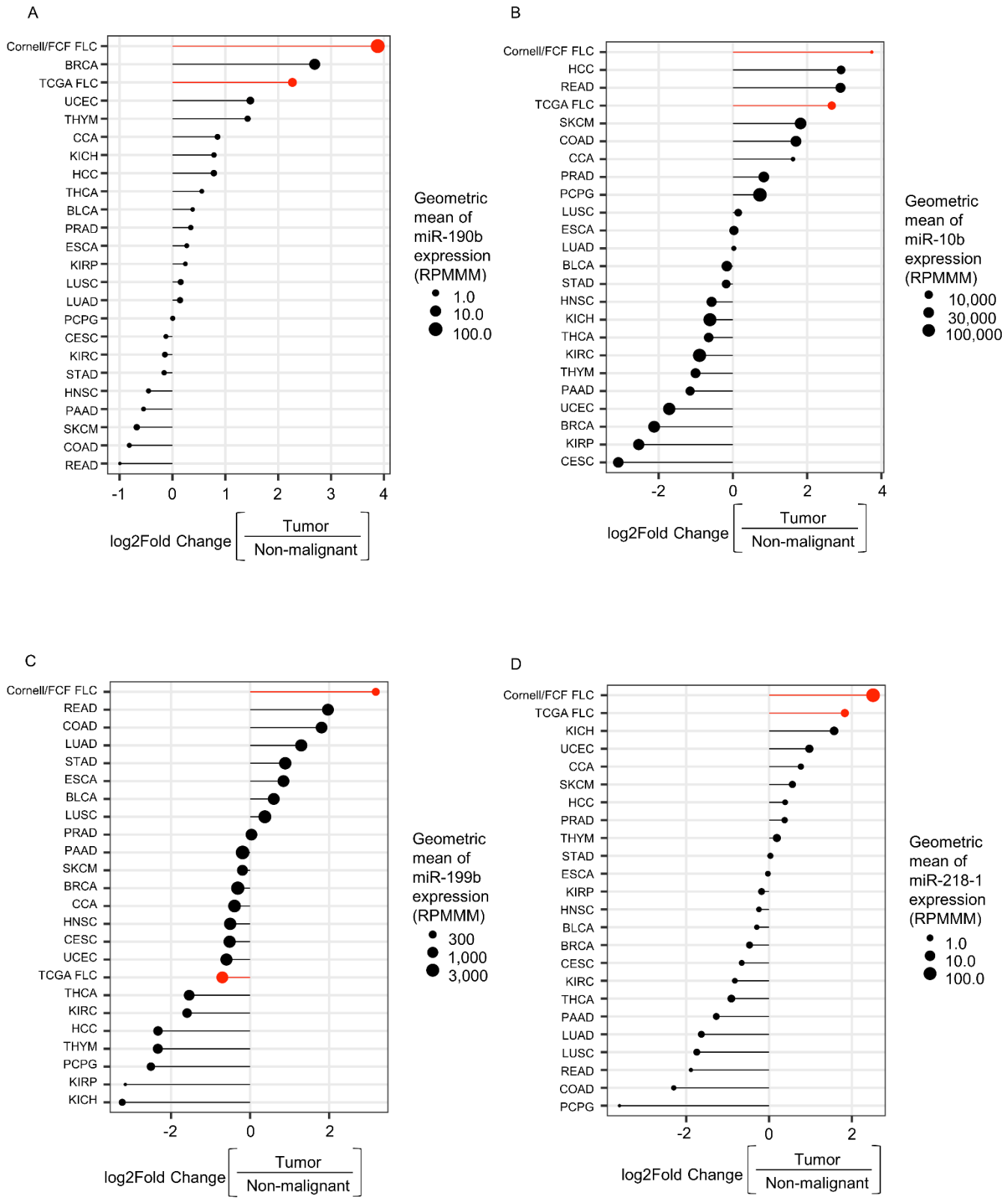
A
Cornell/FCF FLC
BRCA
TCGA FLC
UCEC
THYM
CCA
KICH
HCC
THCA
BLCA
PRAD
ESCA
KIRP
LUSC
LUAD
PCPG
CESC
KIRC
STAD
HNSC
PAAD
SKCM
COAD
READ
-1 0 1 2 3 4
log2Fold Change [Tumor / Non-malignant]
Geometric mean of miR-190b expression (RPMMM)
1.0
10.0
100.0
B
Cornell/FCF FLC
HCC
READ
TCGA FLC
SKCM
COAD
CCA
PRAD
PCPG
LUSC
ESCA
LUAD
BLCA
STAD
HNSC
KICH
THCA
KIRC
THYM
PAAD
UCEC
BRCA
KIRP
CESC
-2 0 2 4
log2Fold Change [Tumor / Non-malignant]
Geometric mean of miR-10b expression (RPMMM)
10,000
30,000
100,000
C
Cornell/FCF FLC
READ
COAD
LUAD
STAD
ESCA
BLCA
LUSC
PRAD
PAAD
SKCM
BRCA
CCA
HNSC
CESC
UCEC
TCGA FLC
THCA
KIRC
HCC
THYM
PCPG
KIRP
KICH
-2 0 2
log2Fold Change [Tumor / Non-malignant]
Geometric mean of miR-199b expression (RPMMM)
300
1,000
3,000
D
Cornell/FCF FLC
TCGA FLC
KICH
UCEC
CCA
SKCM
HCC
PRAD
THYM
STAD
ESCA
KIRP
HNSC
BLCA
BRCA
CESC
KIRC
THCA
PAAD
LUAD
LUSC
READ
COAD
PCPG
-2 0 2
log2Fold Change [Tumor / Non-malignant]
Geometric mean of miR-218-1 expression (RPMMM)
1.0
10.0
100.0

Figure 4. FLC microRNA expression compared to other cancer types. (A-D) Log2 FC expression of the 4 most up-regulated microRNAs in FLC (after removing isomiRs) within TCGA. The size of each circle represents the geometric mean of microRNA expression in each tumor type. Each tumor type is ranked on the y-axis by the log2 FC of the geometric mean of tumor expression relative to non-tumor expression. The FLC sample set used in this study (Cornell/FCF) and the FLC sample set available from TCGA (n=6) are highlighted in red. BLCA, bladder urothelial carcinoma; BRCA, breast invasive carcinoma; CESC, cervical squamous cell and endocervical adenocarcinoma; CCA, cholangiocarcinoma; COAD, colon adenocarcinoma; Cornell/FCF FCL, fibrolamellar carcinoma samples analyzed in this study; ESCA, esophageal carcinoma; HCC, hepatocellular carcinoma; HNSC, head and neck squamous cell carcinoma; KICH, kidney chromophobe; KIRC, kidney renal papillary cell carcinoma; KIRP, kidney renal clear cell carcinoma; LUAD, lung adenocarcinoma; LUSC, lung squamous cell carcinoma, PAAD, pancreatic adenocarcinoma; PCPG, pheochromocytoma and paraganglioma; PRAD, prostate adenocarcinoma; READ, rectum adenocarcinoma; SKCM, skin cutaneous melanoma; STAD, stomach adenocarcinoma; TCGA FLC; fibrolamellar carcinoma; THCA, thyroid carcinoma; THYM, thymoma; UCEC, uterine corpus endometrial carcinoma; RPMMM = Reads per million mapped to microRNAs.

Figure 5

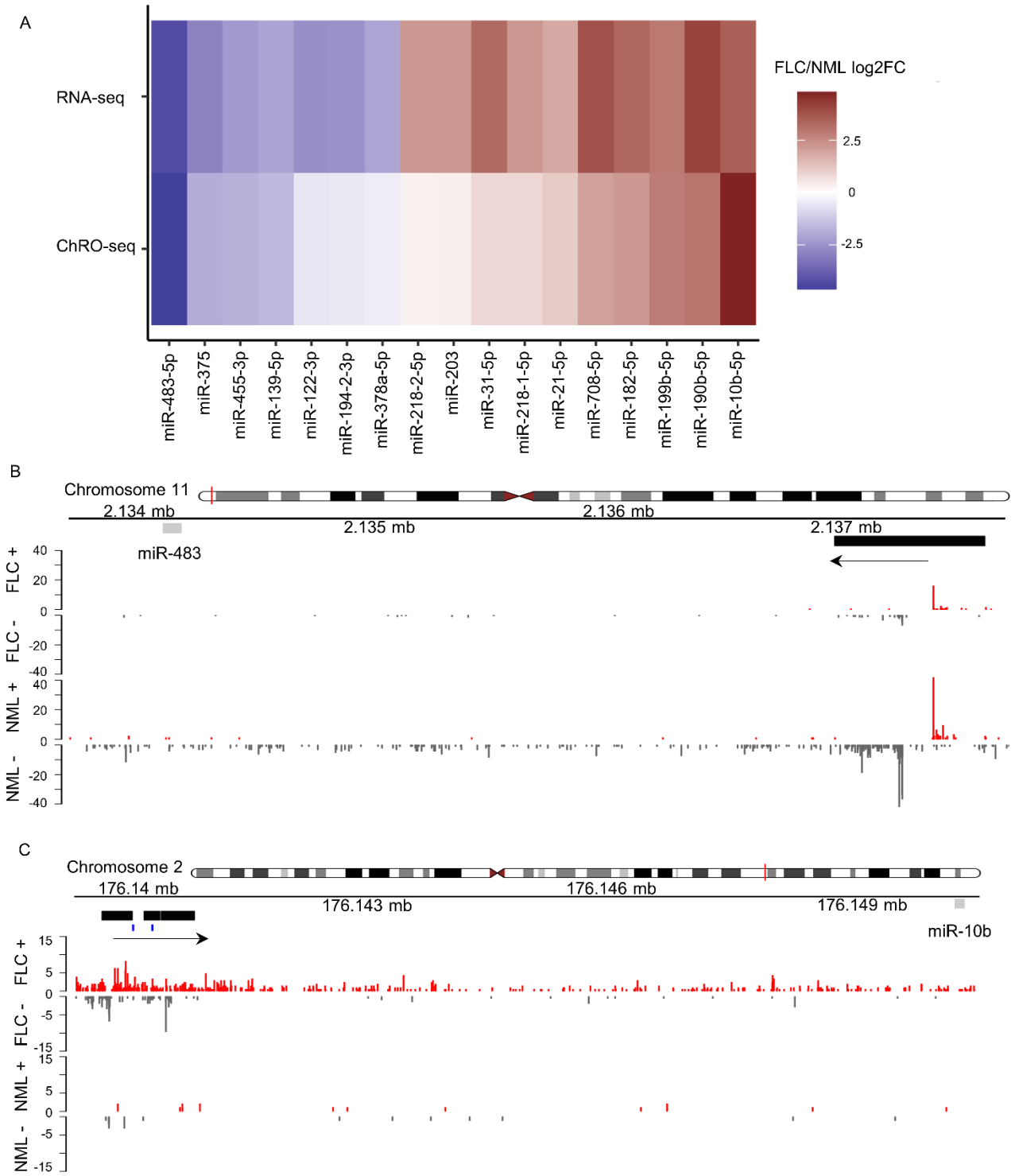
A
RNA-seq
ChRO-seq
FLC/NML log2FC
2.5
0
-2.5
miR-483-5p
miR-375
miR-455-3p
miR-139-5p
miR-122-3p
miR-194-2-3p
miR-378a-5p
miR-218-2-5p
miR-203
miR-31-5p
miR-218-1-5p
miR-21-5p
miR-708-5p
miR-182-5p
miR-199b-5p
miR-190b-5p
miR-10b-5p
B
Chromosome 11
2.134 mb
2.135 mb
2.136 mb
2.137 mb
miR-483
FLC +
FLC -
NML +
NML -
C
Chromosome 2
176.14 mb
176.143 mb
176.146 mb
176.149 mb
miR-10b

Figure 5. miR-10b is the most transcriptionally activated microRNA in FLC. (A) Gene expression (RNA-seq signal, n=19, top row) or transcriptional activity (ChRO-seq signal, n=13, bottom row) for the 17 significantly differentially expressed microRNAs (after removing isomiRs) is shown as the log2 FC in FLC vs NML. **(B)** miR-483-5p and **(C)** miR-10b-5p genome browser tracks showing normalized ChRO-seq signal. The upper and lower panel show the activity in FLC and NML. Activity on the plus and minus strand are shown in red and gray, respectively. The mature microRNA sequence is shown as a grey rectangle, the promoter region of the miRNA is shown as a black rectangle, and the direction of transcription is identified by an arrow. Predicted FOXQ1 bindings sites in the miR-10b promoter are identified by blue dashes.

Figure 6

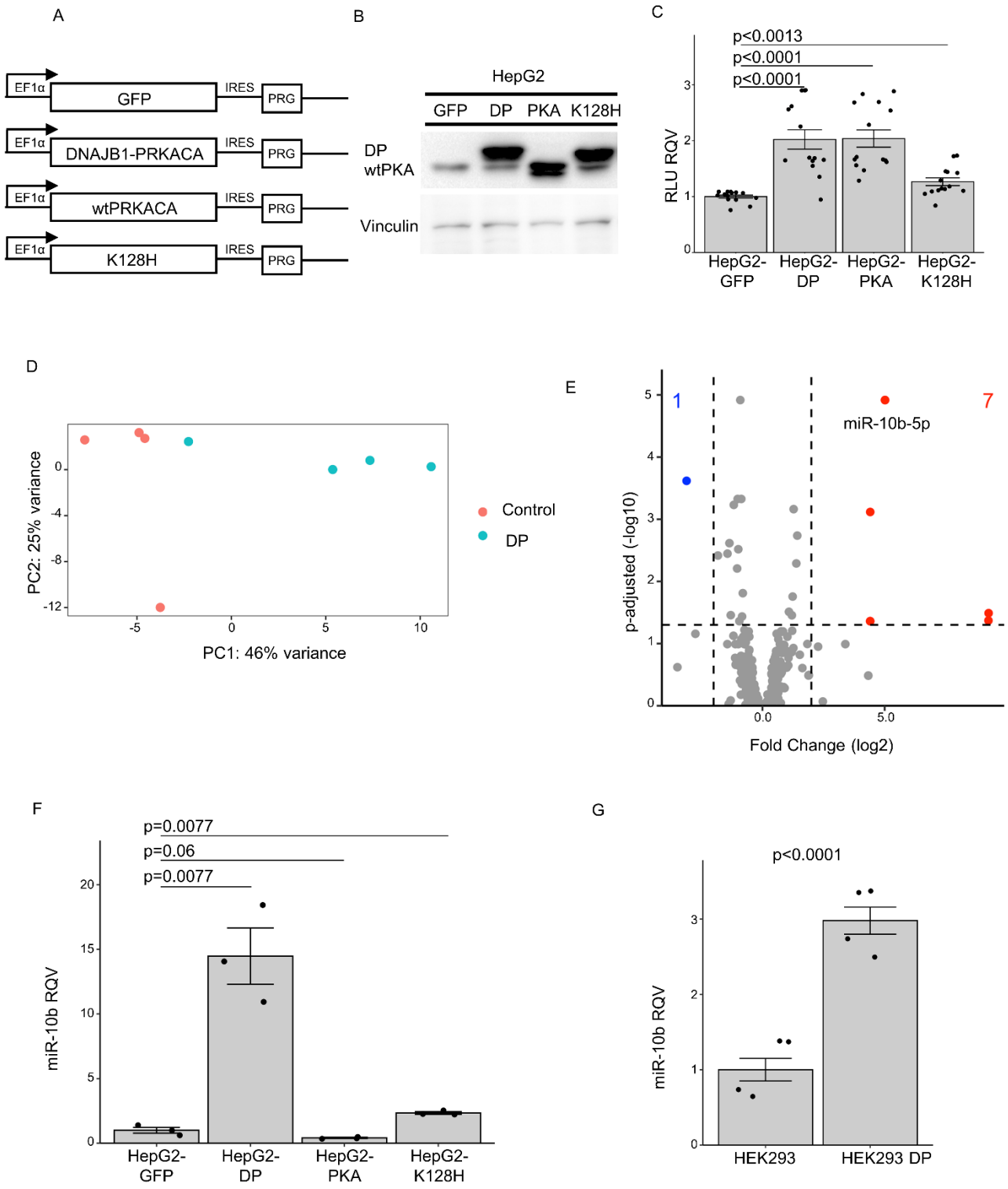
A
EF1α
GFP
IRES
PRG
EF1α
DNAJB1-PRKACA
IRES
PRG
EF1α
wtPRKACA
IRES
PRG
EF1α
K128H
IRES
PRG
B
HepG2
GFP DP PKA K128H
DP
wtPKA
Vinculin
C
p<0.0013
p<0.0001
p<0.0001
RLU RQV
HepG2-GFP
HepG2-DP
HepG2-PKA
HepG2-K128H
D
PC2: 25% variance
PC1: 46% variance
Control
DP
E
1
7
miR-10b-5p
p-adjusted (-log10)
Fold Change (log2)
F
p=0.0077
p=0.06
p=0.0077
miR-10b RQV
HepG2-GFP
HepG2-DP
HepG2-PKA
HepG2-K128H
G
p<0.0001
miR-10b RQV
HEK293
HEK293 DP

Figure 6. DP activity promotes the expression of miR-10b in human but not mouse models. (A) Diagram of expression cassettes for lentiviral constructs. EF1α; human EF1α gene promoter; GFP, green fluorescent protein; DNAJB1-PRCACA, FLC fusion oncogene; wild-type PRKACA; protein kinase A catalytic α subunit; DNAJB1-PRCACA K128H, FLC fusion oncogene containing a lysine-to-histidine substitution at amino acid position 128; IRES, internal ribosome entry site; PRG, puromycin resistance gene. **(B)** Protein expression in HepG2 cell lines detected with a protein kinase A catalytic α subunit (PKAc) antibody. Wild-type PKAc and DP are identified. Lane 1, HepG2-GFP; lane 2, HepG2-DP; lane 3, HepG2-PKA; lane 4, HepG2-K128H. Vinculin expression for loading control is shown in the lower panel. Disclaimer: uncropped immunoblot shown in Supplemental Figure 4A, B. **(C)** Luciferase relative light units (RLU), proportional to viable cells, is shown relative to the HepG2-GFP cell line (2 trials, n=14 each condition). **(D)** Principal component analysis of the log transformed normalized counts from small RNA-sequencing of HepG2-DP (DP, n=3) and HepG2-GFP (control, n=3) samples, in blue and red. **(E)** Volcano plot showing the differentially expressed microRNAs in HepG2-DP relative to HepG2-GFP (only microRNAs with average HepG2-DP or HepG2-GFP expression > 100 shown). Dashed lines represent the log2 (fold change) of expression -2/+2 (vertical) and adjusted *P*=0.05 (horizontal). Up- or down-regulated microRNAs are colored red or blue. **(F)** Quantitative PCR showing the relative quantitative value (RQV) for miR-10b expression in HepG2-GFP, HepG2-DP, HepG2-PKA, and HepG2-K128H cell lines (n=3 each). **(G)** Quantitative PCR for showing the relative quantitative value (RQV) for miR-10b expression in HEK293 and HEK293-DP cell lines (n=4 each). In all assays, each dot represents the average signal of a biological replicate. *P*-values are calculated by two-tailed Student's t-test. *P*-values reported in panels C and F were adjusted for multiple testing correction post-hoc by benjamini-hochberg method.

Figure 7

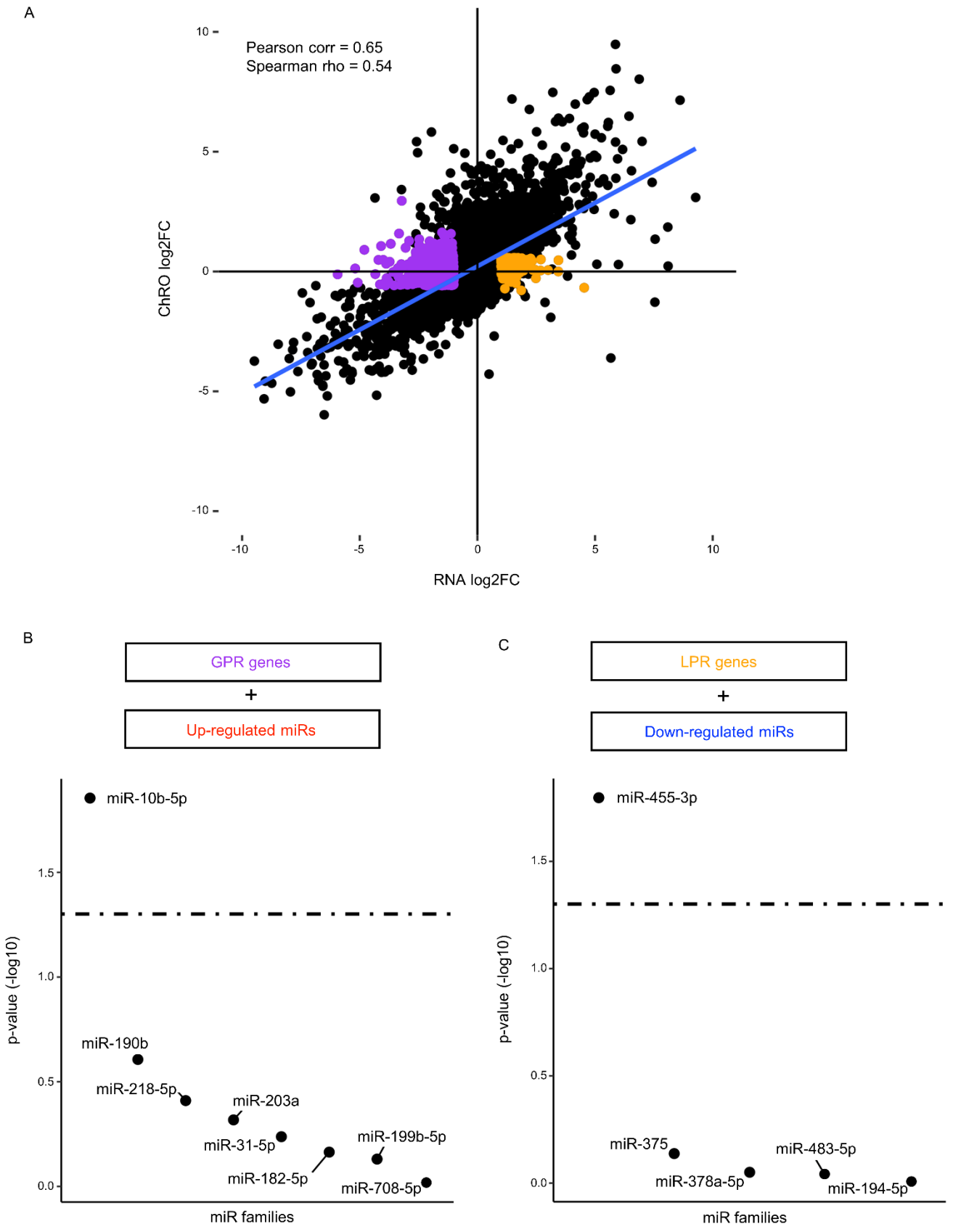
A
Pearson corr = 0.65
Spearman rho = 0.54
ChRO log2FC
RNA log2FC
10
5
0
-5
-10
B
GPR genes
+
Up-regulated miRs
miR-10b-5p
miR-190b
miR-218-5p
miR-203a
miR-31-5p
miR-182-5p
miR-199b-5p
miR-708-5p
p-value (-log10)
miR families
C
LPR genes
+
Down-regulated miRs
miR-455-3p
miR-375
miR-378a-5p
miR-483-5p
miR-194-5p
p-value (-log10)
miR families

Figure 7. miR-10b and miR-455 are master regulators of gene expression in FLC. (A) Scatter plot showing the log2 FC of RNA-seq normalized reads on the x-axis and the log2 FC of ChRO-seq normalized reads on the y-axis for genes in FLC relative to NML. Those genes subject primarily to gain of post-transcriptional regulation (normalized reads > 1000, RNA-seq log2 FC < 1, RNA-seq Padj < 0.05, ChRO-seq log2FC < +/- 0.59, ChRO-seq Padj > 0.2) are highlighted in purple and genes subject primarily to loss of post-transcriptional regulation (normalized reads > 1000, RNA-seq log2 FC > 1, RNA-seq Padj < 0.05, ChRO-seq log2FC < +/- 0.59, ChRO-seq Padj > 0.2) are highlighted in orange. **(B)** Ranked -log10 (*P*-value) of miRhub simulation results. Gain of post-transcriptional regulation genes were examined for enrichment of binding sites for microRNAs up-regulated in FLC (only those microRNAs with predictions in TargetScan included). The dashed line represents *P*-value = 0.05. **(C)** Ranked -log10 (*P*-value) of miRhub simulation results. Loss of post-transcriptional regulation genes were examined for enrichment of binding sites for microRNAs down-regulated in FLC (only those microRNAs with predictions in TargetScan included). The dashed line represents *P*-value = 0.05.

Figure 8

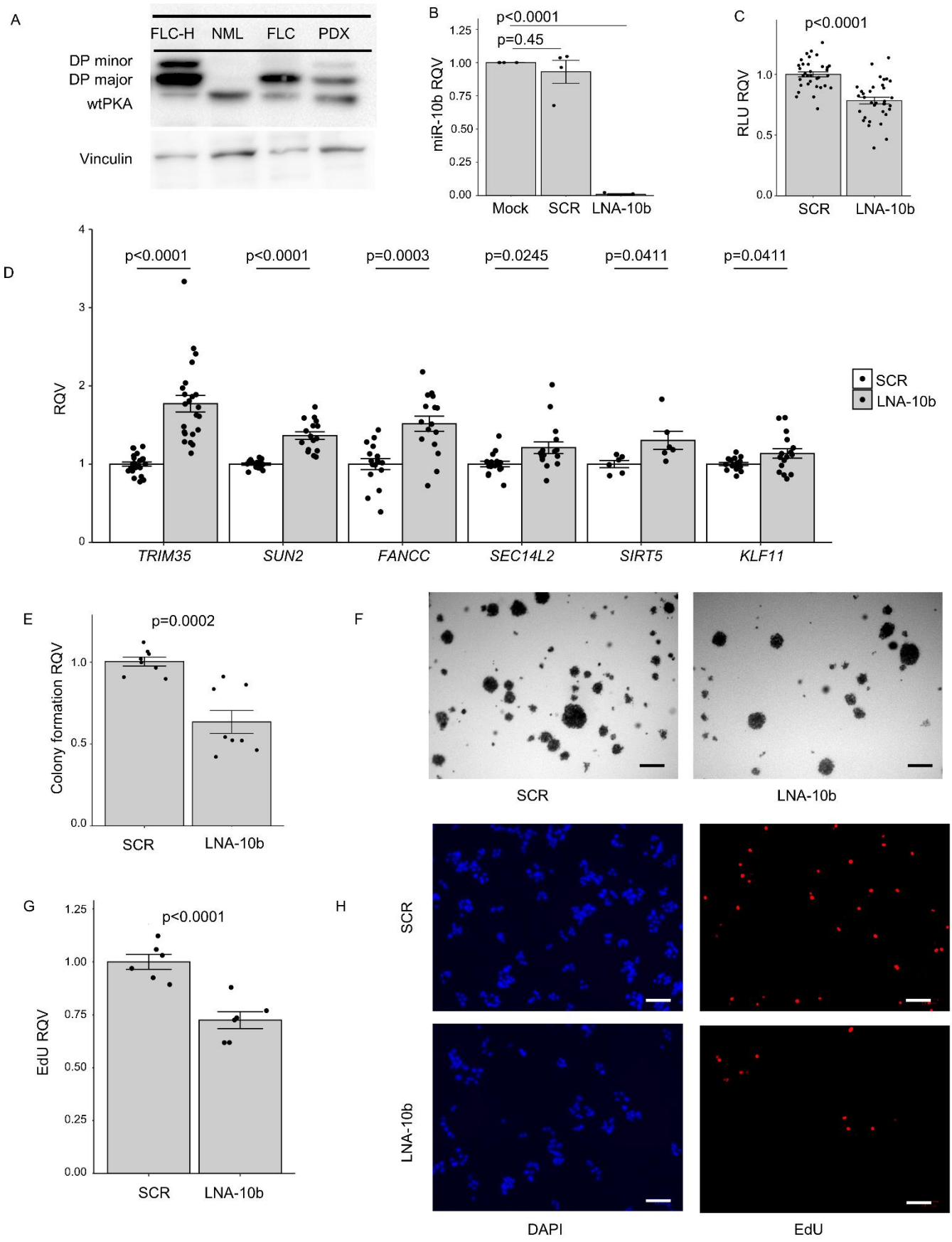
A
FLC-H
NML
FLC
PDX
DP minor
DP major
wtPKA
Vinculin
B
p<0.0001
p=0.45
miR-10b RQV
Mock
SCR
LNA-10b
C
p<0.0001
RLU RQV
SCR
LNA-10b
D
p<0.0001
p<0.0001
p=0.0003
p=0.0245
p=0.0411
p=0.0411
RQV
TRIM35
SUN2
FANCC
SEC14L2
SIRT5
KLF11
SCR
LNA-10b
E
p=0.0002
Colony formation RQV
SCR
LNA-10b
F
SCR
LNA-10b
G
p<0.0001
EdU RQV
SCR
LNA-10b
H
SCR
LNA-10b
DAPI
EdU

Figure 8 miR-10b inhibition reduces FLC cell metabolic activity and proliferation. (A) Protein expression of DNAJB1-PRKACA (DP) is detected with a protein kinase A catalytic α subunit (PKAc) antibody. Wild-type PKAc, DP major, and DP minor are identified. Lane 1, FLC-H cell line; lane 2, Non-malignant liver; lane 3, FLC patient sample; lane 4, FLC patient derived xenograft (PDX) sample. Vinculin expression for loading control is shown in the lower panel. Disclaimer: uncropped immunoblot shown in Supplemental Figure 4A, B. **(B)** Quantitative PCR showing the RQV of miR-10b in FLC-H cells 6 days after 500nM treatment with miR-10b LNA or scrambled sequence compared to mock (n=4 each condition). **(C)** Luciferase signal (RLU) in FLC-H cells after 6 days of 500nM miR-10b LNA treatment is shown as RQV compared to the scrambled negative control (6 trials, n=6 each condition). **(D)** Quantitative PCR showing the RQV of *FANCC*, *KLF11*, *SEC14L2*, *SIRT5*, *SUN2*, and *TRIM35* in FLC-H cells after 6 days of 500nM miR-10b LNA treatment compared to the negative control (n=7-5 trials with 3 replicates for each condition, *SIRT5* n=2 trials). **(E)** Soft agar colony formation of FLC-H cells 35 days after 500nM miR-10b LNA compared to the negative control shown as RQV. **(F)** Representative nitro blue tetrazolium stained images shown (2 trials, n=8 each condition). **(G)** EdU incorporation in FLC-H cells 6 days after 500nM treatment with miR-10b LNA compared to the negative control shown as RQV (2 trials, n=6 each condition). **(H)** Representative DAPI and EdU stained images show total and proliferative cells, respectively. Scale bars equal 100 μM. In all assays, each dot represents the average signal across technical replicates for a single biological replicate. *P*-values are calculated by two-tailed Student's t-test. *P*-values reported in panels B and D were adjusted for multiple testing correction post-hoc by benjamini-hochberg method.

Supplemental Figure 1

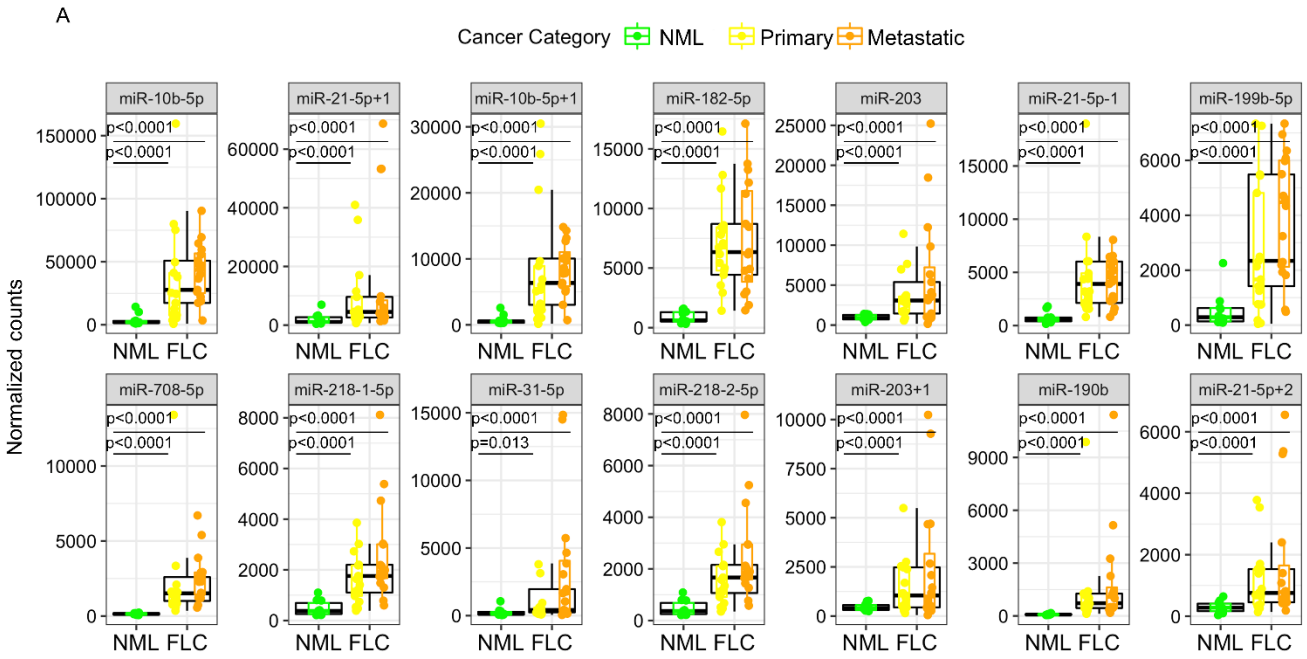

Supplemental Figure 1. Expression of the up-regulated microRNAs in primary and metastatic FLC patient samples. The normalized read counts of each up-regulated microRNA in either primary or metastatic. Each data point represents a patient sample. *P*-values are calculated by two-tailed Student's t-test.

Supplemental Figure 2

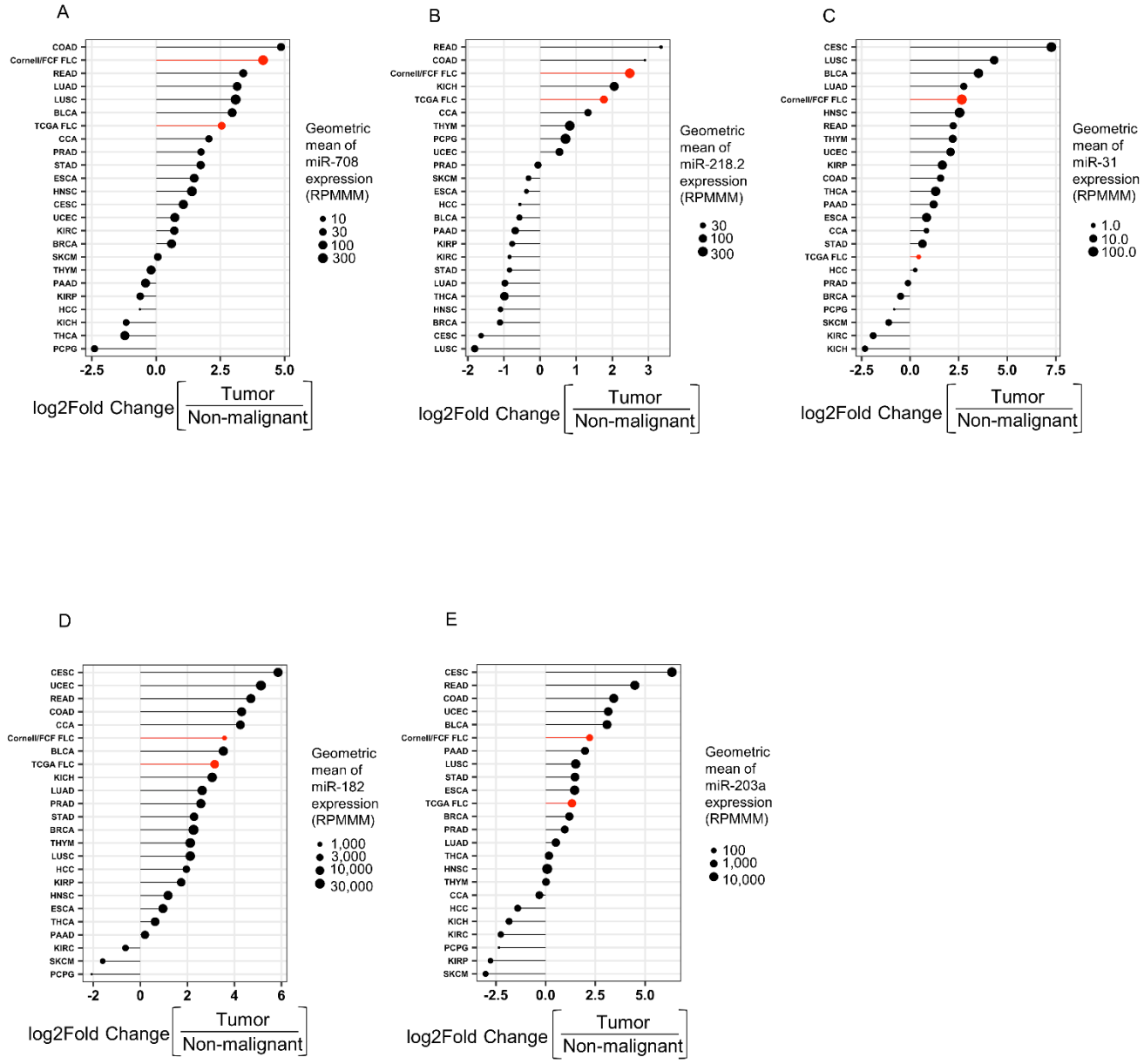

Supplemental Figure 2. FLC microRNA expression compared to other cancer types. (A-E) Log2 FC expression of the 5 next most up-regulated microRNAs in FLC (after removing isomiRs) within TCGA. The size of each circle represents the geometric mean of microRNA expression in each tumor type. Each tumor type is ranked on the y-axis by the log2 FC of the geometric mean of tumor expression relative to non-tumor expression. The FLC sample set used in this study (Cornell/FCF) and the FLC sample set available from TCGA (n=6) are highlighted in red. BLCA, bladder urothelial carcinoma; BRCA, breast invasive carcinoma; CESC, cervical squamous cell and endocervical adenocarcinoma; CCA, cholangiocarcinoma; COAD, colon adenocarcinoma; Cornell/FCF FCL, fibrolamellar carcinoma samples analyzed in this study; ESCA, esophageal carcinoma; HCC, hepatocellular carcinoma; HNSC, head and neck squamous cell carcinoma; KICH, kidney chromophobe; KIRC, kidney renal papillary cell carcinoma; KIRP, kidney renal clear cell carcinoma; LUAD, lung adenocarcinoma; LUSC, lung squamous cell carcinoma, PAAD, pancreatic adenocarcinoma; PCPG, pheochromocytoma and paraganglioma; PRAD, prostate adenocarcinoma; READ, rectum adenocarcinoma; SKCM, skin cutaneous melanoma; STAD, stomach adenocarcinoma; TCGA FLC; fibrolamellar carcinoma; THCA, thyroid carcinoma; THYM, thymoma; UCEC, uterine corpus endometrial carcinoma; RPMMM = Reads per million mapped to microRNAs.

Supplemental Figure 3

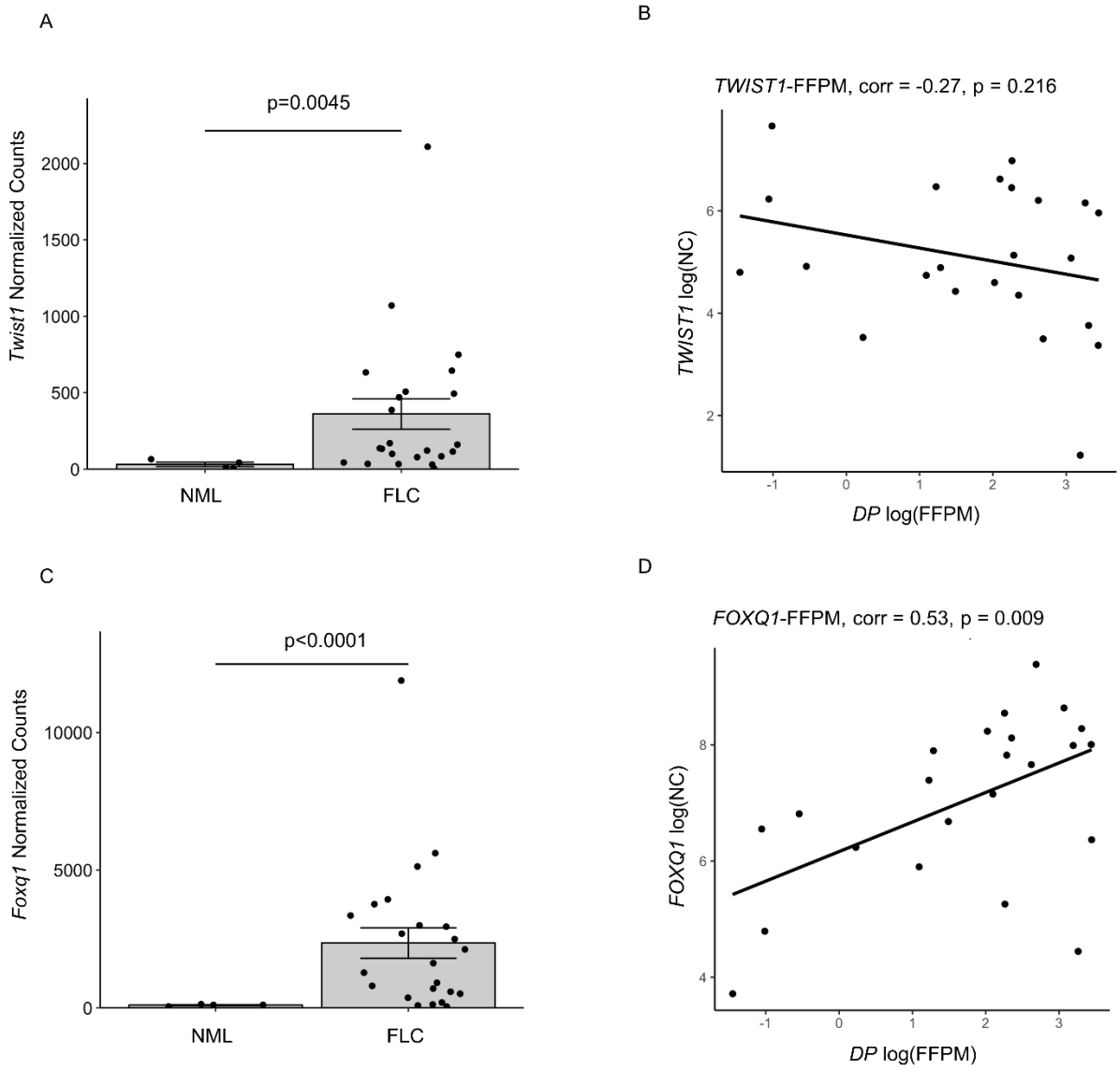

Supplemental Figure 3. FOXQ1 mRNA levels correlates to DP expression. (A) Bar graph showing the normalized RNA-seq read counts for *TWIST1* in NML and FLC. **(B)** Correlation of *TWIST1* (y-axis) and *DP* (x-axis). **(C)** Bar graph showing the normalized RNA-seq normalized read counts for *FOXQ1* in NML and FLC. **(D)** Correlation of *FOXQ1* (y-axis) and *DP* (x-axis). Expression shown as the log of normalized counts in FLC samples with RNA-seq data (n=19). Measurements from individual samples are shown as data points. *P*-values calculated by two-tailed Student's t-test.

Supplemental Figure 4

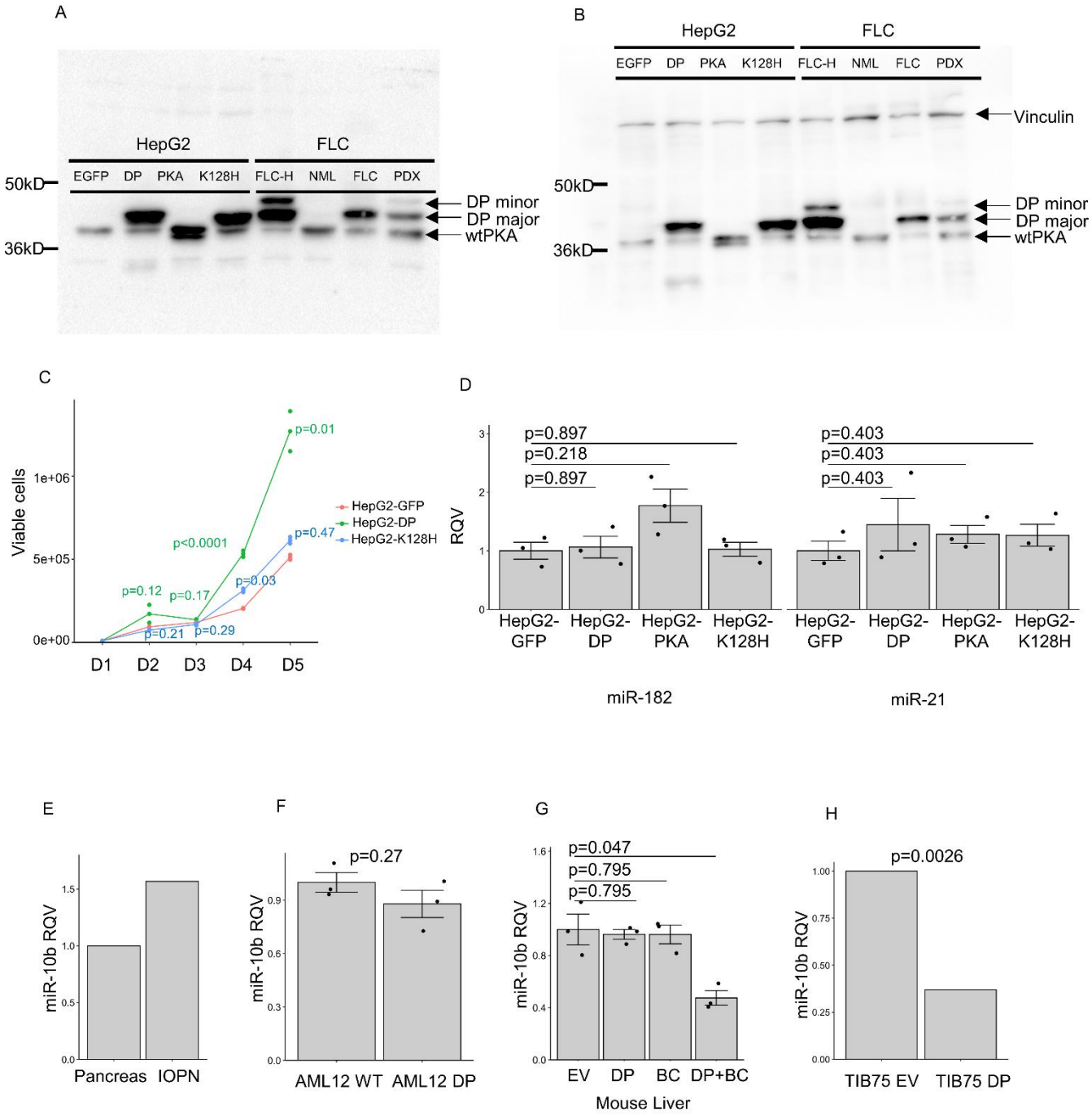

Supplemental Figure 4. (A) Immunoblot probed with a PKAc antibody. Wild-type PKAc and DP are identified. Lane 1, HepG2-GFP; lane 2, HepG2-DP; lane 3, HepG2-PKA; lane 4, HepG2-K128H; lane 5, FLC-H cell line; lane 6, non-malignant liver (NML) sample; lane 7, Fibrolamellar carcinoma (FLC) sample; lane 8, patient-derived xenograft (PDX) sample. Molecular masses from the ladder of 36 and 50 kilodaltons are denoted. **(B)** Immunoblot from panel A probed with vinculin antibody. Disclaimer: cropped content of immunoblot is shown in Figure 6B and Figure 8A. **(C)** Growth of HepG2-GFP, HepG2-DP, and HepG2-K128H cell lines over 5 days (n=3 each line). **(D)** Quantitative PCR showing the RQV of miR-10b in an intraductal oncocytic papillary neoplasm (IOPN) sample relative to healthy pancreatic tissue (Pancreas) (n=1). **(E)** Quantitative PCR showing the RQV of miR-182 and miR-21 expression in HepG2-GFP, HepG2-DP, HepG2-PKA, and HepG2-K128H cell lines (n=3 each line). **(F)** Quantitative PCR showing the RQV of miR-10b in AML12 wild type (WT) and DNAJB1-PRKACA over-expression (DP) cell lines (n=3 each line). **(G)** Quantitative PCR showing the RQV of miR-10b in mouse livers transposed with empty vector (EV), DNAJB1-PRKACA expression (DP), constitutively active β-catenin expression (BC), or DNAJB1-PRKACA and constitutively active β-catenin expression (DP+BC) (n=3 each condition). **(H)** Quantitative PCR showing the RQV of miR-10b in TIB75 empty vector (EV) and DNAJB1-PRKACA over-expression (DP) cell lines. In all assays, each dot represents the average signal across technical replicates for a single biological replicate. *P*-values calculated by two-tailed Student's t-test. *P*-values reported in panels D and G were adjusted for multiple testing correction post-hoc by benjamini-hochberg method.

Supplemental Figure 5

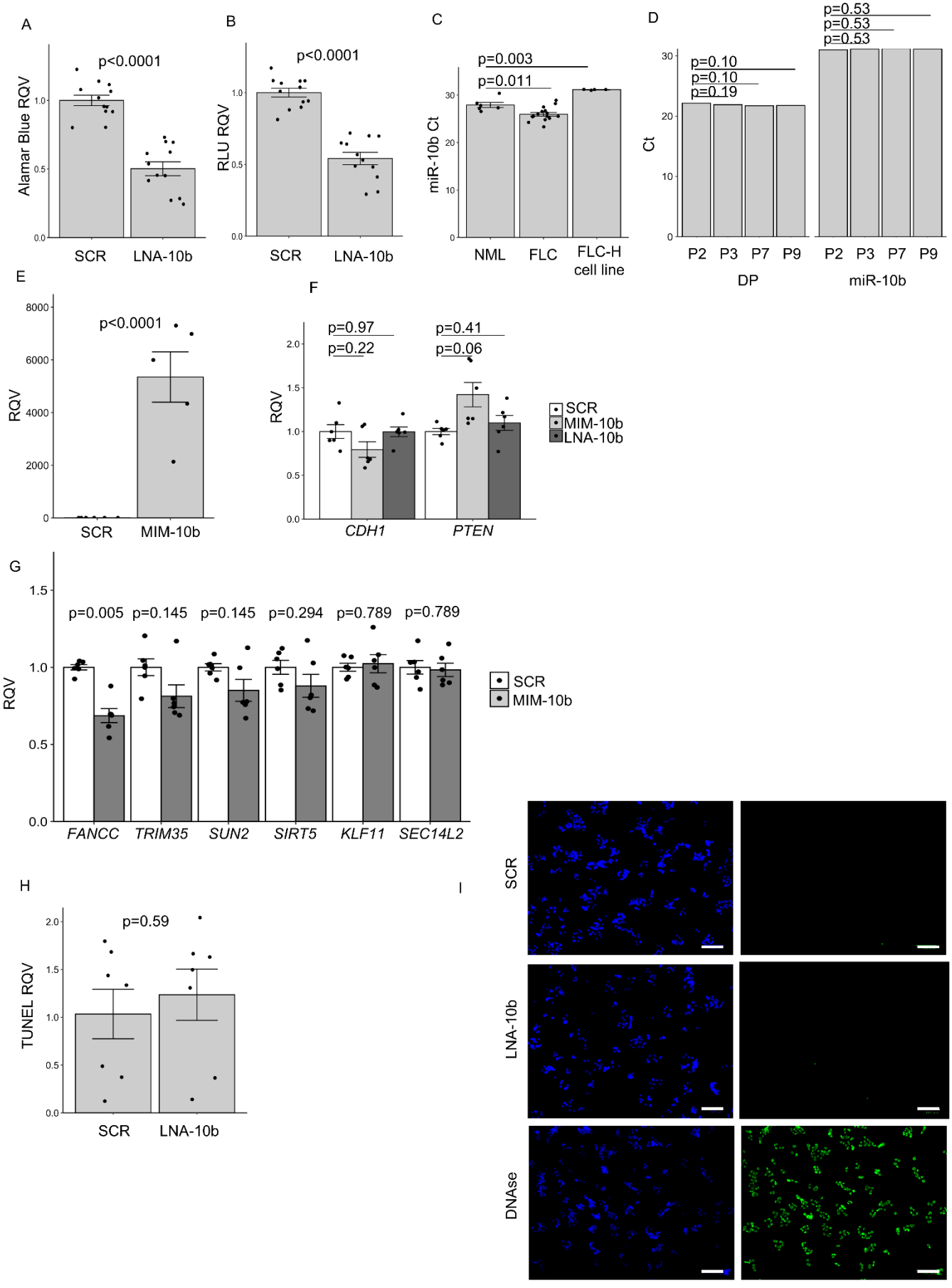

Supplemental Figure 5. (A) Alamar blue absorbance and **(B)** luciferase relative light unit (RLU) assays in FLC-C cells after treatment with miR-10b LNA is shown as RQV compared to the negative control (scrambled sequence) 2 days after 100nM treatment. **(C)** Quantitative PCR cycle threshold (Ct) values for miR-10b expression in non-malignant liver (NML), fibrolamellar carcinoma (FLC), and the FLC-H cell line. **(D)** Quantitative PCR cycle threshold (Ct) values for DP and miR-10b expression in FLC-H cell passage 2, 3, 7, and 9 (P2-P9). **(E)** Quantitative PCR showing the RQV of miR-10b in FLC-H cells 6 days after 500nM treatment with miR-10b mimic (MIM-10b) or scrambled sequence compared to mock (2 trials, n=6 each condition). **(F)** Quantitative PCR showing the RQV of *CDH1* and *PTEN* in FLC-H cells 6 days after 500nM treatment with miR-10b mimic (MIM-10b), miR-10b inhibitor (LNA-10b), or scrambled sequence compared to mock (2 trials, n=6 each condition). **(G)** Quantitative PCR showing the RQV of *FANCC, TRIM35, SUN2, SIRT5, KLF11,* and *SEC14L2* in FLC-H cells after 6 days of 500nM miR-10b MIM treatment compared to the negative control (2 trials, n=6 in each condition). **(H)** TUNEL assay in FLC-H cells 6 days after 500nM treatment with miR-10b LNA compared to the negative control shown as RQV (2 trials, n=7 in each condition). **(I)** Representative DAPI and TUNEL stained images show total and apoptotic cells in scramble and miR-10b LNA treated cells. After fixation a subset of cells were treated with DNase to provide a positive control for the staining reaction. Scale bars equal 100 μM. In all assays, each dot represents the average signal across technical replicates for a single biological replicate. *P*-values calculated by two-tailed Student's t-test. *P*-values reported in panels C, D, F and G were adjusted for multiple testing correction post-hoc by benjamini-hochberg method.

Supplemental Table 1. **FLC patient information**

Sample type (non-malignant liver, primary, metastatic), location of tumor, patient age, patient gender, and confirmation of *DNAJB1-PRKACA* fusion is listed for each patient (which was given an anonymous alpha-numeric identifier). *DNAJB1-PRKACA* was detected by either quantitative PCR, STARFusion analysis of RNA-seq libraries, or western blot of tumor samples. For qPCR, a cycle threshold of less than 33.5 was considered positive for *DNAJB1-PRKACA* expression. For samples analyzed in prior studies, the PMID reference is listed.

Supplemental Table 2. Small RNA sequencing information

Mapping statistics for the small RNA-sequencing data. Samples not included in study were excluded due to being a duplicate tissue sample or failure to detect DP in a FLC sample. Metrics include total reads, trimmed reads, reads excluded due to small size following trimming (<14nt; Too Short Reads), reads perfectly aligning to the genome (Exact Match Reads) reads containing at least 1 mismatch (Mismatch Reads), reads mapped to microRNA loci (miR Mapped), reads mapped to tRNA loci (tRNA Mapped), and reads mapped to yRNA loci (yRNA Mapped).

References

1. Graham RP, Torbenson MS. Fibrolamellar carcinoma: A histologically unique tumor with unique molecular findings. *Semin Diagn Pathol.* 2017;34(2):146-152.
2. Graham RP, Yeh MM, Lam-Himlin D, et al. Molecular testing for the clinical diagnosis of fibrolamellar carcinoma. *Mod Pathol.* 2018;31(1):141-149.
3. Graham RP, Craig JR, Jin L, et al. Environmental exposures as a risk factor for fibrolamellar carcinoma. *Mod Pathol.* 2017;30(6):892-896.
4. Kassahun WT. Contemporary management of fibrolamellar hepatocellular carcinoma: diagnosis, treatment, outcome, prognostic factors, and recent developments. *World J Surg Oncol.* 2016;14(1):151.
5. Mayo SC, Mavros MN, Nathan H, et al. Treatment and prognosis of patients with fibrolamellar hepatocellular carcinoma: a national perspective. *J Am Coll Surg.* 2014;218(2):196-205.
6. Ramai D, Ofosu A, Lai JK, Gao ZH, Adler DG. Fibrolamellar Hepatocellular Carcinoma: A Population-Based Observational Study. *Dig Dis Sci.* 2021;66(1):308-314.
7. Eggert T, McGlynn KA, Duffy A, Manns MP, Greten TF, Altekruse SF. Epidemiology of fibrolamellar hepatocellular carcinoma in the USA, 2000-10. *Gut.* 2013;62(11):1667-1668.
8. Yamashita S, Vauthey JN, Kaseb AO, et al. Prognosis of Fibrolamellar Carcinoma Compared to Non-cirrhotic Conventional Hepatocellular Carcinoma. *J Gastrointest Surg.* 2016;20(10):1725-1731.
9. Ang CS, Kelley, R.K., Choti, M.A., Cosgrove, D.P., Chou, J.F., Klimstra, D., Torbenson, M.S., Ferrell, L., Pawlik, T.M., Fong, Y., O'Reilly, E.M., Ma, J., McGuire, J., Vallarapu, G.P., Griffin, A., Stipa, F., Capanu, M., DeMatteo, R.P., Venook, A.P., Abou-Alfa, G.K. Clinicopathologic Characteristics and Survival Outcomes of Patients With Fibrolamellar Carcinoma: Data From the Fibrolamellar Carcinoma Consortium. *Gastrointest Cancer Res.* 2013;6:3-9.
10. Honeyman JN, Simon EP, Robine N, et al. Detection of a recurrent DNAJB1-PRKACA chimeric transcript in fibrolamellar hepatocellular carcinoma. *Science.* 2014;343(6174):1010-1014.
11. Xu L, Hazard FK, Zmoos AF, et al. Genomic analysis of fibrolamellar hepatocellular carcinoma. *Hum Mol Genet.* 2015;24(1):50-63.
12. Cornella H, Alsinet C, Sayols S, et al. Unique genomic profile of fibrolamellar hepatocellular carcinoma. *Gastroenterology.* 2015;148(4):806-818 e810.
13. Engelholm LH, Riaz A, Serra D, et al. CRISPR/Cas9 Engineering of Adult Mouse Liver Demonstrates That the Dnajb1-Prkaca Gene Fusion Is Sufficient to Induce Tumors Resembling Fibrolamellar Hepatocellular Carcinoma. *Gastroenterology.* 2017;153(6):1662-1673 e1610.
14. Kastenhuber ER, Lalazar G, Houlihan SL, et al. DNAJB1-PRKACA fusion kinase interacts with beta-catenin and the liver regenerative response to drive fibrolamellar hepatocellular carcinoma. *Proc Natl Acad Sci U S A.* 2017;114(50):13076-13084.
15. Bockus LB, Humphries KM. cAMP-dependent Protein Kinase (PKA) Signaling Is Impaired in the Diabetic Heart. *J Biol Chem.* 2015;290(49):29250-29258.
16. Colombe AS, Pidoux G. Cardiac cAMP-PKA Signaling Compartmentalization in Myocardial Infarction. *Cells.* 2021;10(4).
17. Saad NS, Elnakish MT, Ahmed AAE, Janssen PML. Protein Kinase A as a Promising Target for Heart Failure Drug Development. *Arch Med Res.* 2018;49(8):530-537.
18. Sorenson EC, Khanin R, Bamboat ZM, et al. Genome and transcriptome profiling of fibrolamellar hepatocellular carcinoma demonstrates p53 and IGF2BP1 dysregulation. *PLoS One.* 2017;12(5):e0176562.
19. Dinh TA, Vitucci EC, Wauthier E, et al. Comprehensive analysis of The Cancer Genome Atlas reveals a unique gene and non-coding RNA signature of fibrolamellar carcinoma. *Sci Rep.* 2017;7:44653.
20. Simon EP, Freije CA, Farber BA, et al. Transcriptomic characterization of fibrolamellar hepatocellular carcinoma. *Proc Natl Acad Sci U S A.* 2015;112(44):E5916-5925.
21. Dinh TA, Sritharan R, Smith FD, et al. Hotspots of Aberrant Enhancer Activity in Fibrolamellar Carcinoma Reveal Candidate Oncogenic Pathways and Therapeutic Vulnerabilities. *Cell Rep.* 2020;31(2):107509.
22. Dinh TA, Jewell ML, Kanke M, et al. MicroRNA-375 Suppresses the Growth and Invasion of Fibrolamellar Carcinoma. *Cell Mol Gastroenterol Hepatol.* 2019;7(4):803-817.
23. Farber BA, Requena, D., Bhanot, U.K., Lalazar, G., Simon, E.P., Hammond, W.J., La Quaglia, M.P. and Simon, S.M. Non coding RNA analysis in fibrolamellar hepatocellular carcinoma. *Oncotarget.* 2018;9(12):10211-10227.
24. Bartel DP. Metazoan MicroRNAs. *Cell.* 2018;173(1):20-51.

25. Lv XB, Liu L, Cheng C, et al. SUN2 exerts tumor suppressor functions by suppressing the Warburg effect in lung cancer. *Sci Rep.* 2015;5:17940.
26. Kuo KK, Hsiao PJ, Chang WT, et al. Therapeutic Strategies Targeting Tumor Suppressor Genes in Pancreatic Cancer. *Cancers (Basel).* 2021;13(15).
27. Kennedy RD, Chen CC, Stuckert P, et al. Fanconi anemia pathway-deficient tumor cells are hypersensitive to inhibition of ataxia telangiectasia mutated. *J Clin Invest.* 2007;117(5):1440-1449.
28. Hirano S, Yamamoto K, Ishiai M, et al. Functional relationships of FANCC to homologous recombination, translesion synthesis, and BLM. *EMBO J.* 2005;24(2):418-427.
29. Chen X, Chen Y, Huang HM, et al. SUN2: A potential therapeutic target in cancer. *Oncol Lett.* 2019;17(2):1401-1408.
30. Cheng Y. YC, Li X., Wang X., Chen J., Wang Z. and Xu B. Loss of Sun2 promotes the progression of prostate cancer by regulating fatty acid oxidation. *Oncotarget.* 2017;8(52):89620-89630.
31. Chen Z, Wang Z, Guo W, et al. TRIM35 Interacts with pyruvate kinase isoform M2 to suppress the Warburg effect and tumorigenicity in hepatocellular carcinoma. *Oncogene.* 2015;34(30):3946-3956.
32. Yao L, Zhou Y, Sui Z, et al. HBV-encoded miR-2 functions as an oncogene by downregulating TRIM35 but upregulating RAN in liver cancer cells. *EBioMedicine.* 2019;48:117-129.
33. Kanke M, Baran-Gale J, Villanueva J, Sethupathy P. miRquant 2.0: an Expanded Tool for Accurate Annotation and Quantification of MicroRNAs and their isomiRs from Small RNA-Sequencing Data. *J Integr Bioinform.* 2016;13(5):307.
34. Thomson JM, Newman M, Parker JS, Morin-Kensicki EM, Wright T, Hammond SM. Extensive post-transcriptional regulation of microRNAs and its implications for cancer. *Genes Dev.* 2006;20(16):2202-2207.
35. Li QJ, Zhou L, Yang F, et al. MicroRNA-10b promotes migration and invasion through CADM1 in human hepatocellular carcinoma cells. *Tumour Biol.* 2012;33(5):1455-1465.
36. Datar I, Kalpana G, Choi J, et al. Critical role of miR-10b in B-RafV600E dependent anchorage independent growth and invasion of melanoma cells. *PLoS One.* 2019;14(4):e0204387.
37. Sheedy P, Medarova, Z. The fundamental role of miR-10b in metastatic cancer. *Am J Cancer Res.* 2018;8(9):1674-1688.
38. Grant CE, Bailey TL, Noble WS. FIMO: scanning for occurrences of a given motif. *Bioinformatics.* 2011;27(7):1017-1018.
39. Castro-Mondragon JA, Riudavets-Puig R, Rauluseviciute I, et al. JASPAR 2022: the 9th release of the open-access database of transcription factor binding profiles. *Nucleic Acids Res.* 2022;50(D1):D165-D173.
40. Kim SS, Kycia I, Karski M, et al. DNAJB1-PRKACA in HEK293T cells induces LINC00473 overexpression that depends on PKA signaling. 2021.
41. Vyas M, Hechtman JF, Zhang Y, et al. DNAJB1-PRKACA fusions occur in oncocytic pancreatic and biliary neoplasms and are not specific for fibrolamellar hepatocellular carcinoma. *Mod Pathol.* 2020;33(4):648-656.
42. Turnham RE, Smith FD, Kenerson HL, et al. An acquired scaffolding function of the DNAJ-PKAc fusion contributes to oncogenic signaling in fibrolamellar carcinoma. *Elife.* 2019;8.
43. Baran-Gale J, Fannin EE, Kurtz CL, Sethupathy P. Beta cell 5'-shifted isomiRs are candidate regulatory hubs in type 2 diabetes. *PLoS One.* 2013;8(9):e73240.
44. Oikawa T, Wauthier E, Dinh TA, et al. Model of fibrolamellar hepatocellular carcinomas reveals striking enrichment in cancer stem cells. *Nat Commun.* 2015;6:8070.
45. Ni J, Wen X, Yao J, et al. Tocopherol-associated protein suppresses prostate cancer cell growth by inhibition of the phosphoinositide 3-kinase pathway. *Cancer Res.* 2005;65(21):9807-9816.
46. Lomberk G, Mathison AJ, Grzenda A, et al. Sequence-specific recruitment of heterochromatin protein 1 via interaction with Kruppel-like factor 11, a human transcription factor involved in tumor suppression and metabolic diseases. *J Biol Chem.* 2012;287(16):13026-13039.
47. Yihan L, Xiaojing W, Ao L, et al. SIRT5 functions as a tumor suppressor in renal cell carcinoma by reversing the Warburg effect. *J Transl Med.* 2021;19(1):521.
48. Hu T, Shukla SK, Vernucci E, et al. Metabolic Rewiring by Loss of Sirt5 Promotes Kras-Induced Pancreatic Cancer Progression. *Gastroenterology.* 2021;161(5):1584-1600.
49. Bourguignon LY, Wong G, Earle C, Krueger K, Spevak CC. Hyaluronan-CD44 interaction promotes c-Src-mediated twist signaling, microRNA-10b expression, and RhoA/RhoC up-regulation, leading to Rho-kinase-associated cytoskeleton activation and breast tumor cell invasion. *J Biol Chem.* 2010;285(47):36721-36735.
50. Abdelmaksoud-Dammak R, Chamtouri N, Triki M, et al. Overexpression of miR-10b in colorectal cancer patients: Correlation with TWIST-1 and E-cadherin expression. *Tumour Biol.* 2017;39(3):1010428317695916.
51. Pattabiraman DR, Bierie B, Kober KI, et al. Activation of PKA leads to mesenchymal-to-epithelial transition and loss of tumor-initiating ability. *Science.* 2016;351(6277):aad3680.

52. Firull AB, Conway, S.J. Phosphoregulation of Twist1 Provides a Mechanism of Cell Fate Control. *Current Medicinal Chemistry.* 2008,;15:2641-2647.
53. Abba M, Patil N, Rasheed K, et al. Unraveling the role of FOXQ1 in colorectal cancer metastasis. *Mol Cancer Res.* 2013;11(9):1017-1028.
54. Jia Yun Liu* XYW, Guan Nan Wu, Fu-Kun Liu, Xue-Quan Yao. FOXQ1 promotes cancer metastasis by PI3K/AKT signaling regulation in colorectal carcinoma. *Am J Transl Res.* 2017;9:2207-2218.
55. Bahena-Ocampo I, Espinosa M, Ceballos-Cancino G, et al. miR-10b expression in breast cancer stem cells supports self-renewal through negative PTEN regulation and sustained AKT activation. *EMBO Rep.* 2016;17(5):648-658.
56. Liu J, Zhang J, Li Y, Wang L, Sui B, Dai D. MiR-455-5p acts as a novel tumor suppressor in gastric cancer by down-regulating RAB18. *Gene.* 2016;592(2):308-315.
57. Zhan T, Zhu Q, Han Z, et al. miR-455-3p Functions as a Tumor Suppressor by Restraining Wnt/beta-Catenin Signaling via TAZ in Pancreatic Cancer. *Cancer Manag Res.* 2020;12:1483-1492.
58. Zhao Y, Yan M, Yun Y, et al. MicroRNA-455-3p functions as a tumor suppressor by targeting eIF4E in prostate cancer. *Oncol Rep.* 2017;37(4):2449-2458.
59. Zhan T, Huang X, Tian X, et al. Downregulation of MicroRNA-455-3p Links to Proliferation and Drug Resistance of Pancreatic Cancer Cells via Targeting TAZ. *Mol Ther Nucleic Acids.* 2018;10:215-226.